Supporting Information

Development of Rhodamine 6G Based Fluorescent Chemosensors for Al^{3+} Ion Detection: Effect of Ring Strain and Substituent in Enhancing Its Sensing Performance

Jayanta Mandal,[a] Pravat Ghorai,[a] Kunal Pal,[b] Tanurima Bhaumik,[a] Parimal Karmakar [b] and Amrita Saha[*a]

[a]*Department of Chemistry, Jadavpur University, Kolkata- 700032, India.*

E-mail: asaha@chemistry.jdvu.ac.in; amritasahachemju@gmail.com; Tel. +91-33-24572146

[b]*Department of Life Science and Biotechnology, Jadavpur University, Kolkata-700032, India.*

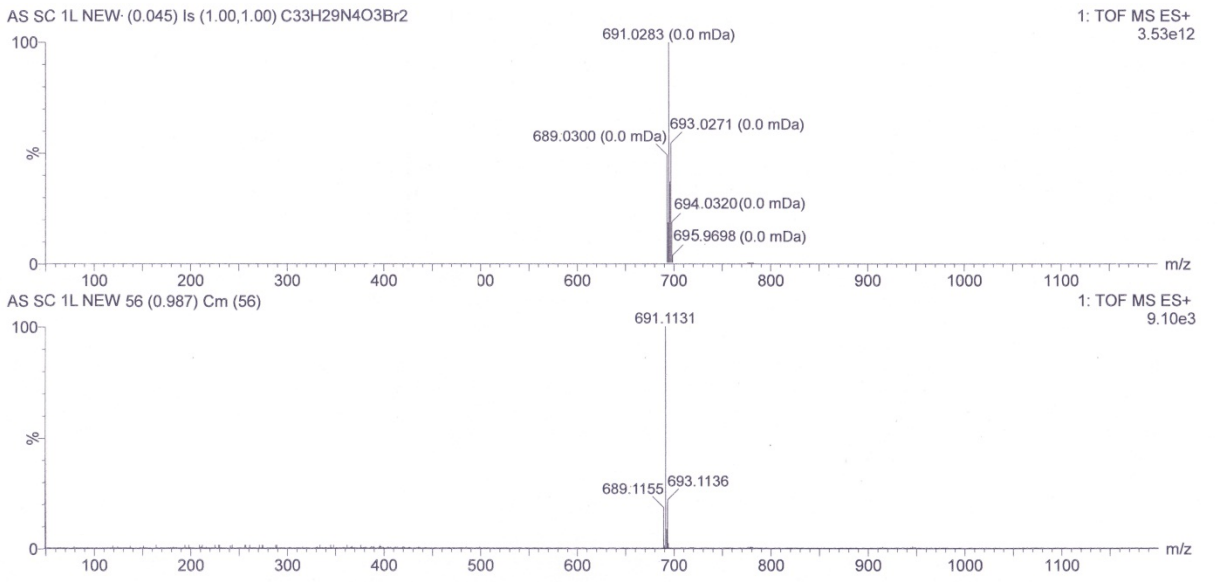

Figure S1. ESI-mass spectrum of chemosensor **H_3L1** (above is simulated pattern and below is experimental finding).

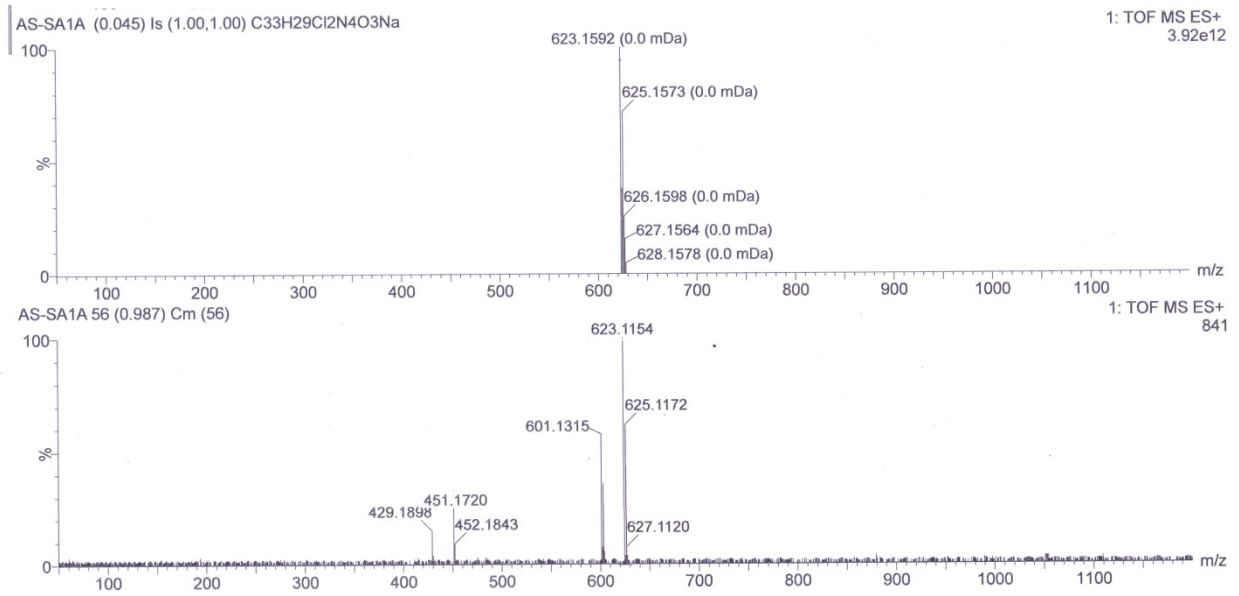

Figure S2. ESI-mass spectrum of chemosensor **H_3L2** (above is simulated pattern and below is experimental finding).

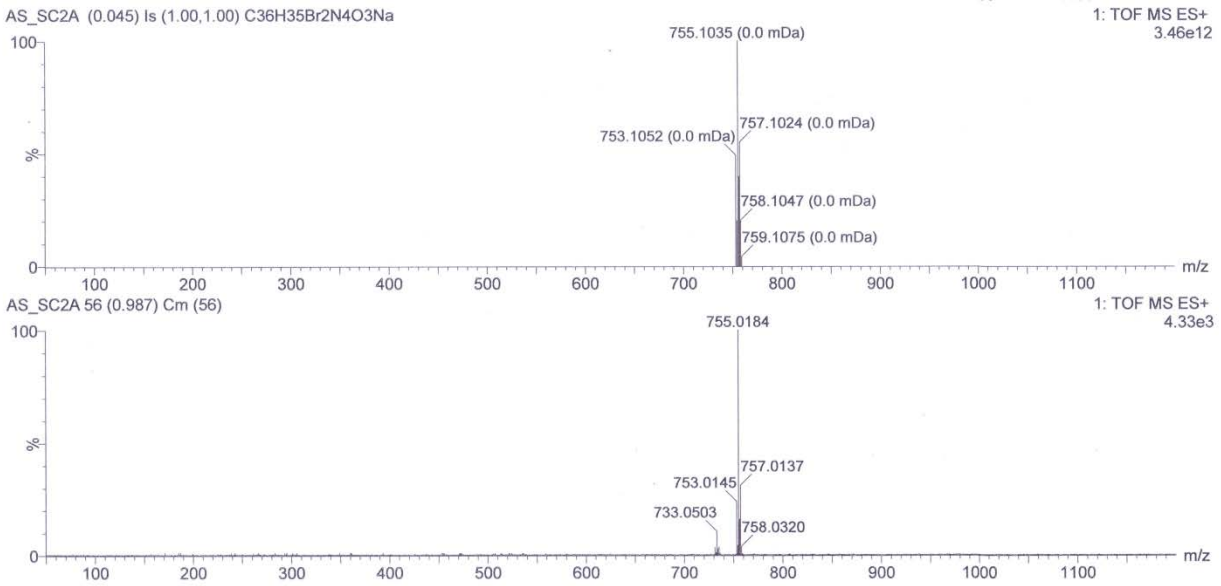

Figure S3. ESI-mass spectrum of chemosensor **H_3L3** (above is simulated pattern and below is experimental finding).

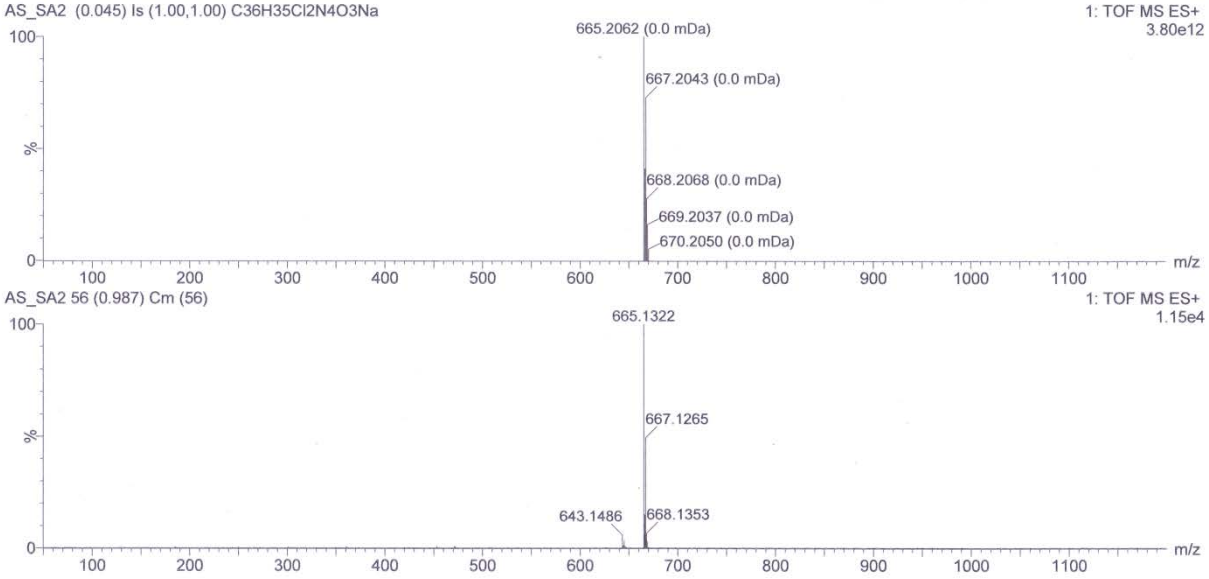

Figure S4. ESI-mass spectrum of chemosensor **H_3L4** (above is simulated pattern and below is experimental finding).

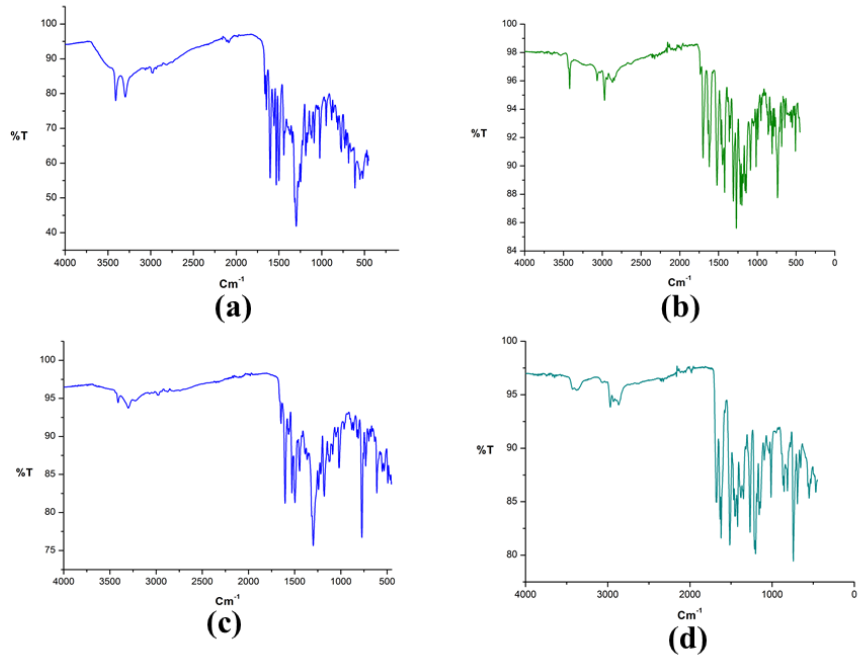

Figure S5. FTIR spectra of chemosensors **(a) H_3L1, (b) H_3L2, (c) H_3L3** and **(d) H_3L4**.

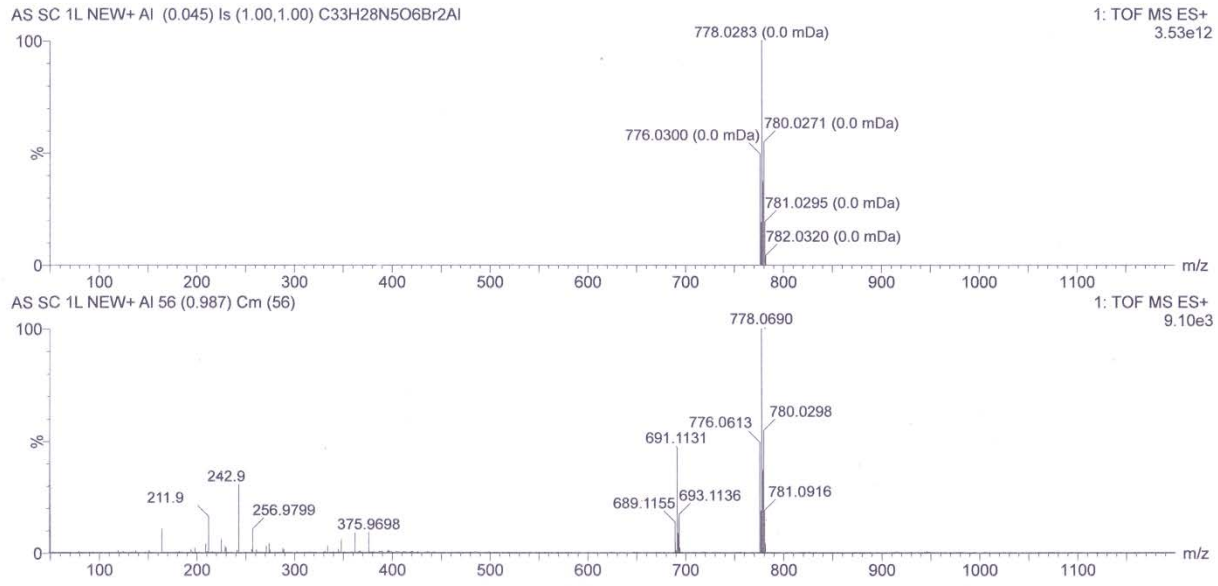

Figure S6. ESI-mass spectrum of complex **1** (above is simulated pattern and below is experimental finding).

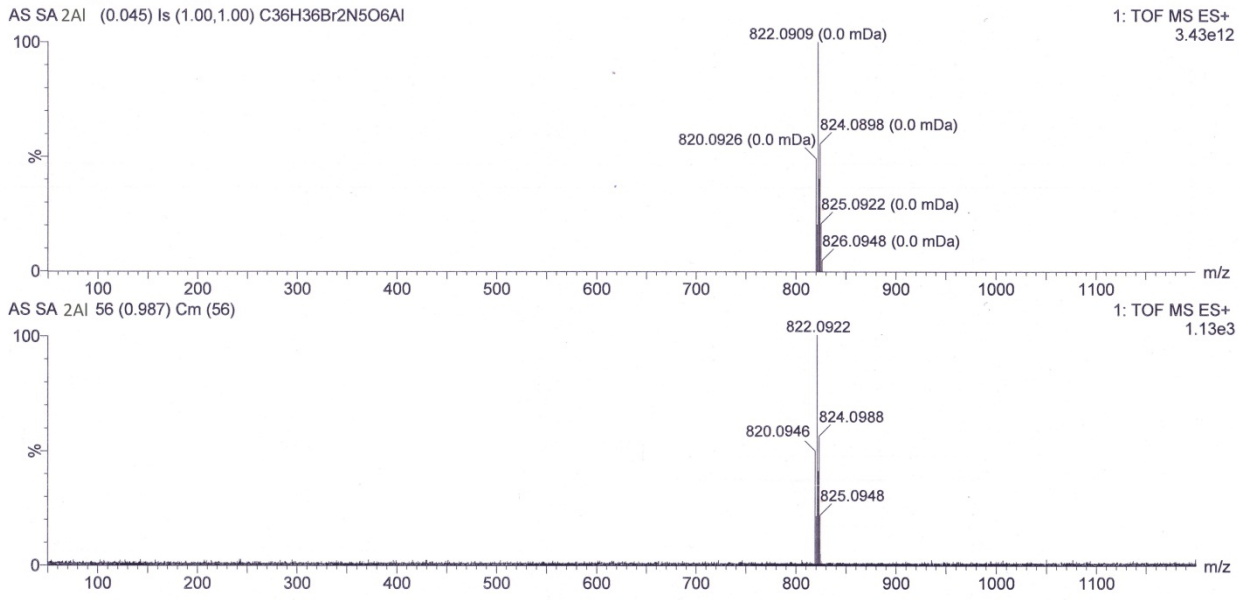

Figure S7. ESI-mass spectrum of complex **2** (above is simulated pattern and below is experimental finding).

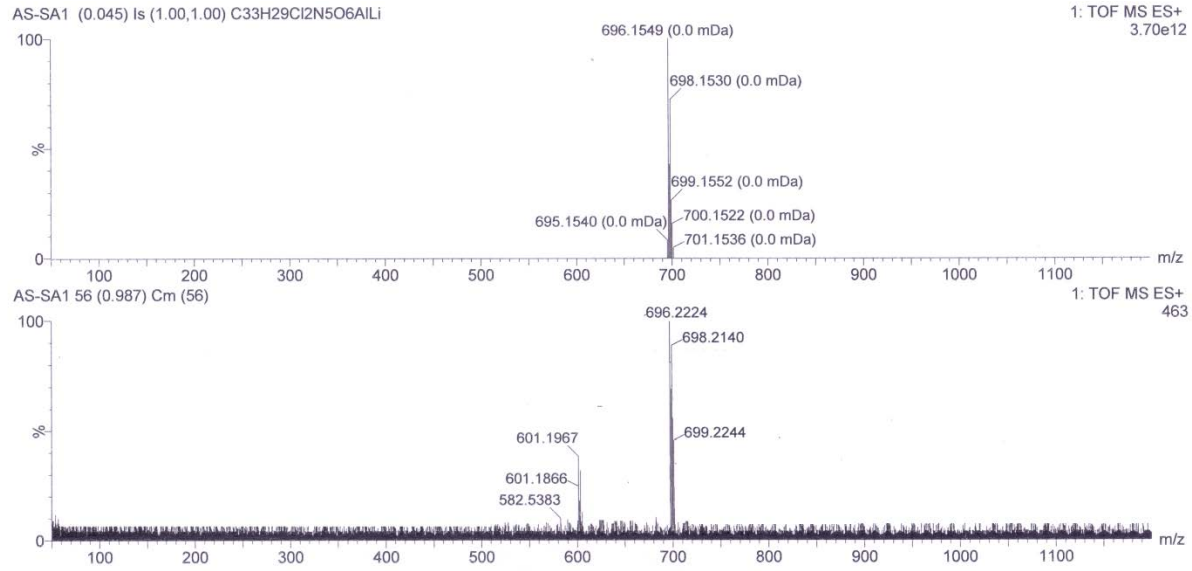

Figure S8. ESI-mass spectrum of complex **3** (above is simulated pattern and below is experimental finding).

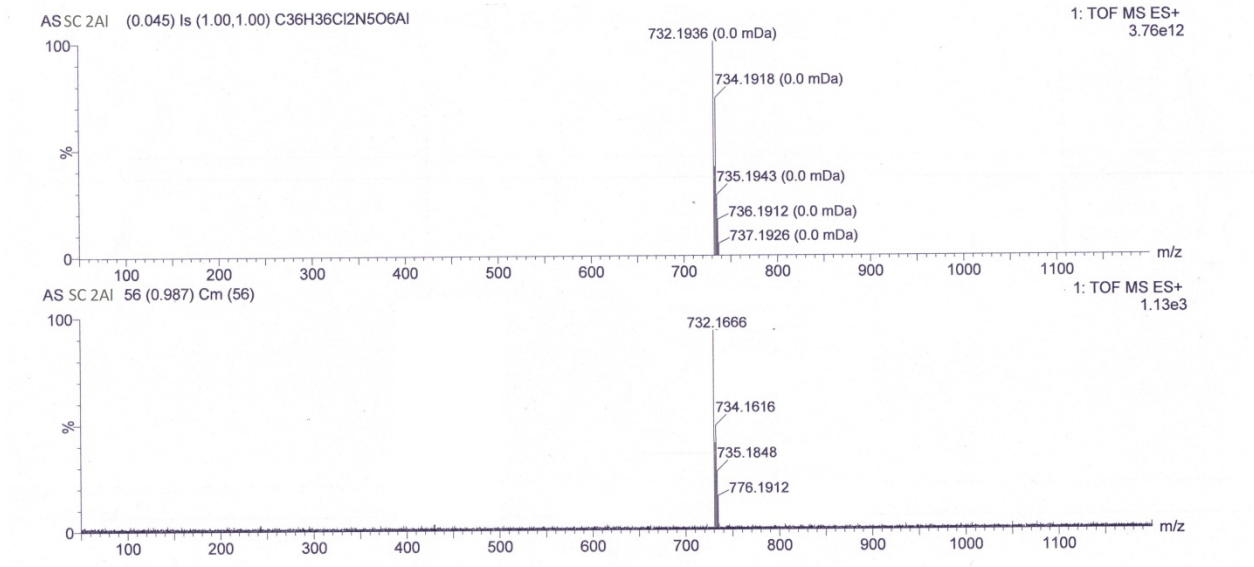

Figure S9. ESI-mass spectrum of complex **4** (above is simulated pattern and below is experimental finding).

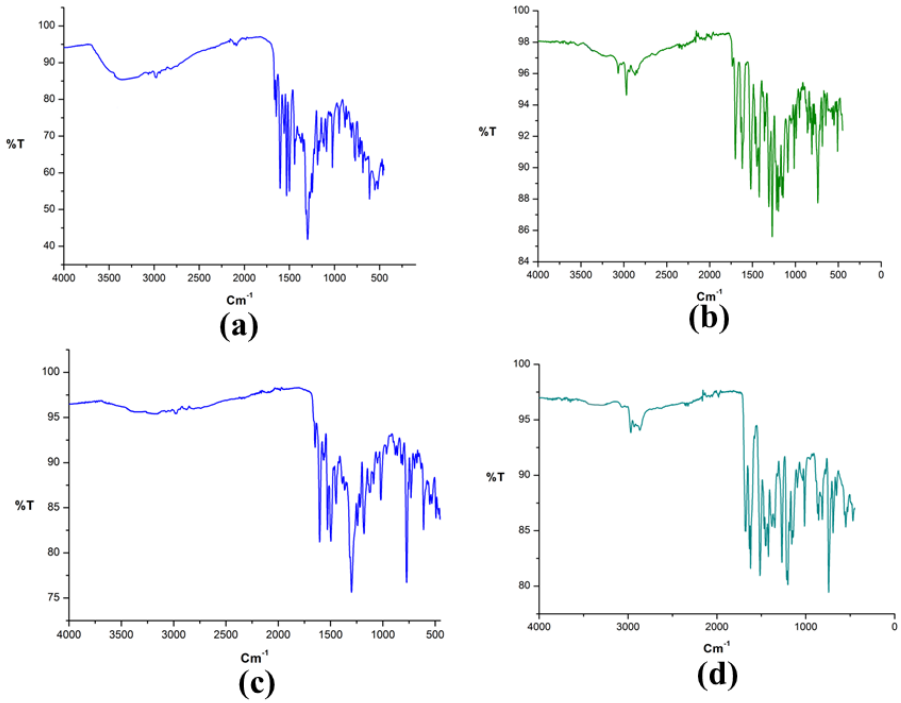

Figure S10. FTIR spectra of **(a)** complex 1**, (b)** complex 2**, (c)** complex 3 and **(d)** complex 4**.**

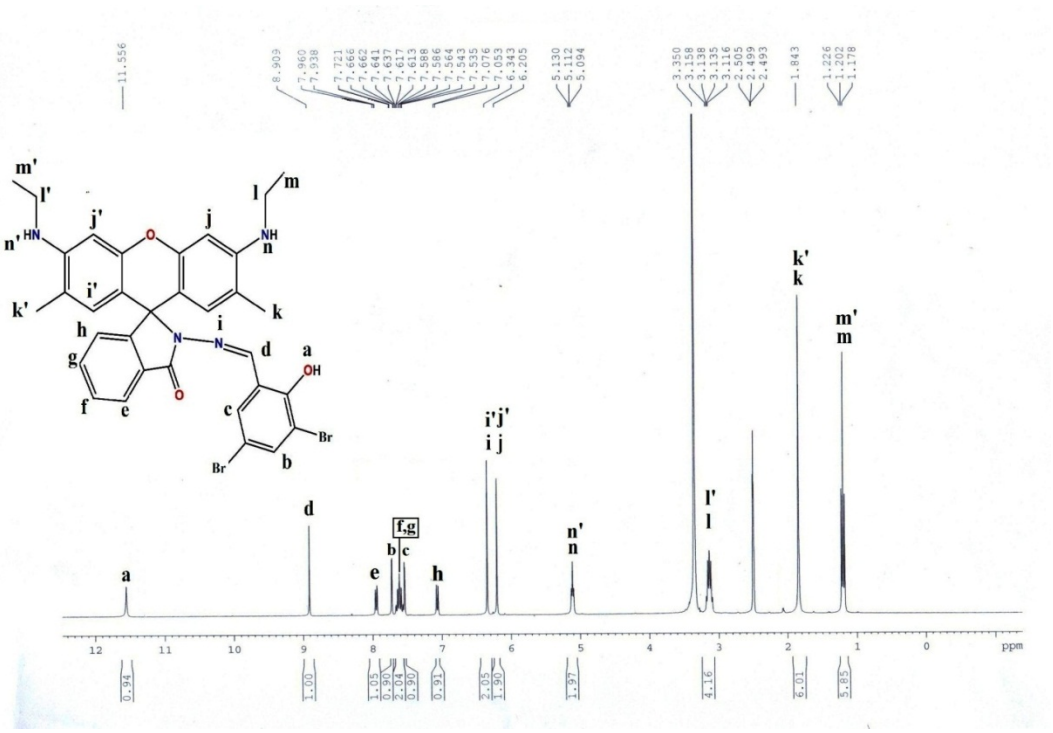

Figure S11. [1]H-NMR of the chemosensor **H_3L1** in DMSO-d_6 recorded on a 400 MHz Bruker NMR spectrometer.

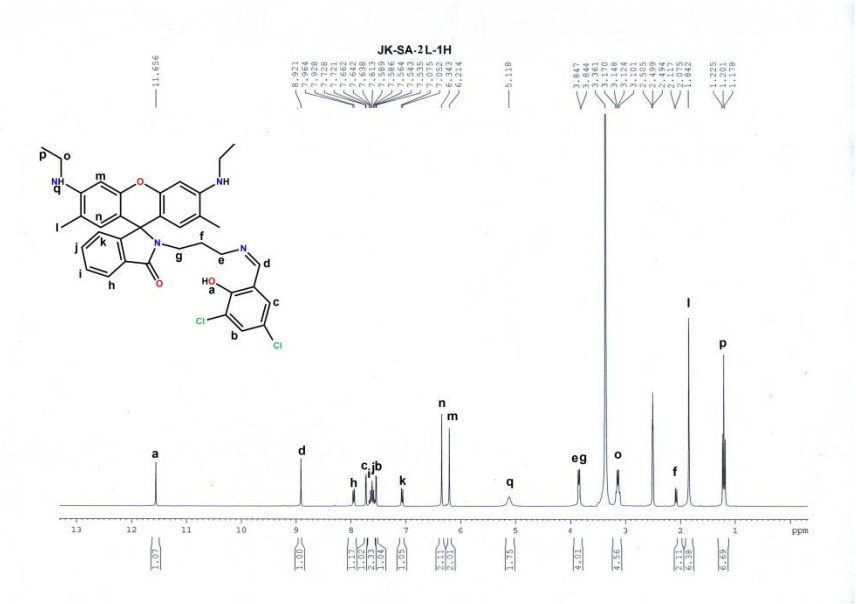

Figure S12. [1]H-NMR of the free ligand **H_3L2** in DMSO-d_6 recorded on a 400 MHz Bruker NMR spectrometer.

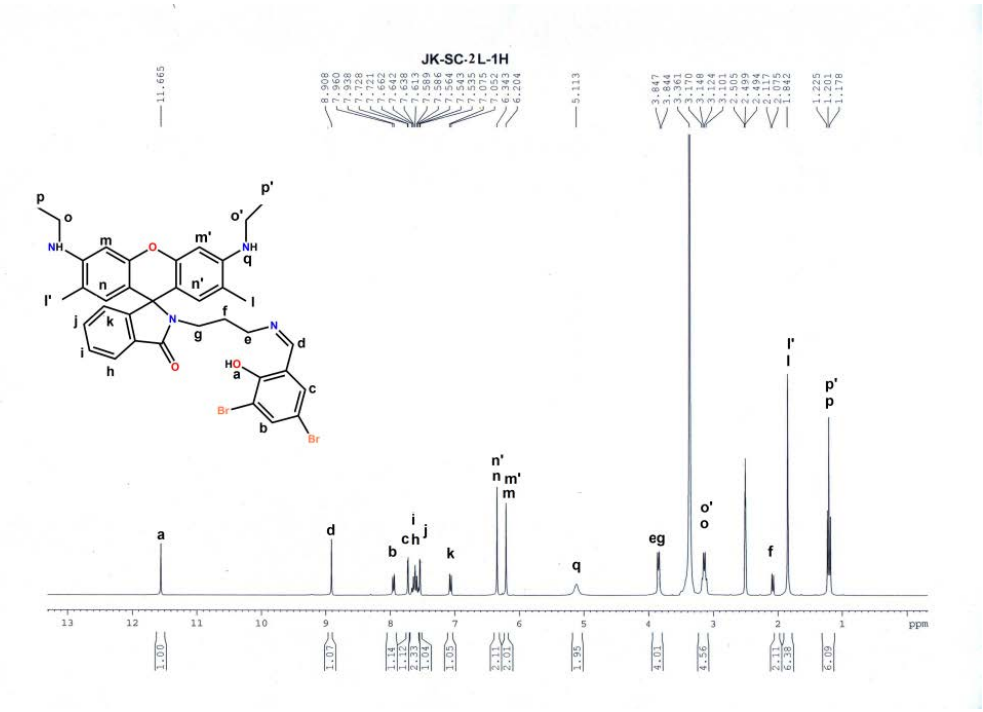

Figure S13. ^{1}H-NMR of the free ligand **H_3L3** in DMSO-d_6 recorded on a 400 MHz Bruker NMR spectrometer.

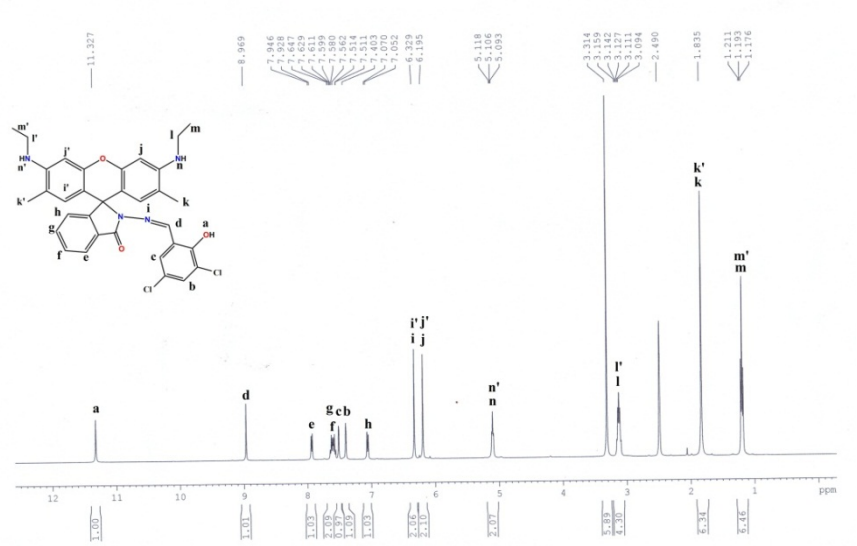

Figure S14. ^{1}H-NMR of the free ligand **H_3L4** in DMSO-d_6 recorded on a 400 MHz Bruker NMR spectrometer

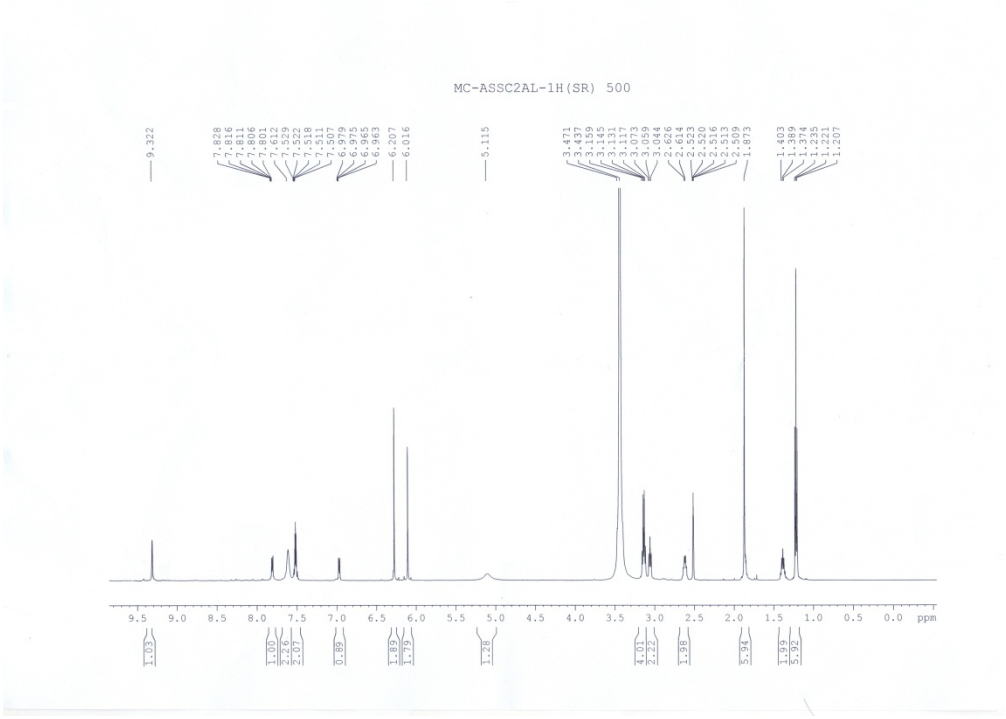

Figure S15. ^{1}H-NMR of the complex **1** in DMSO-d_6 recorded on a 400 MHz Bruker NMR spectrometer

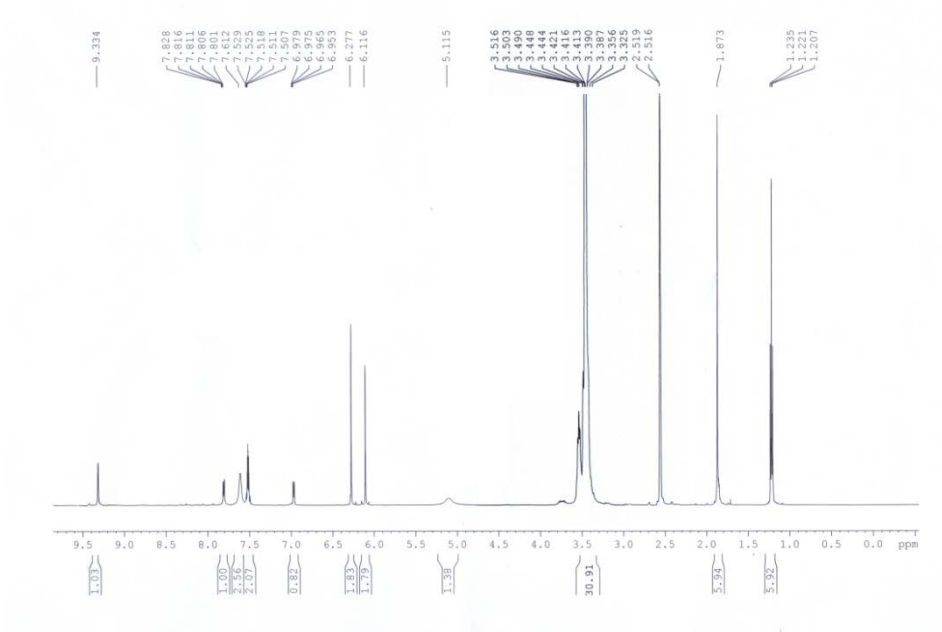

Figure S16. ^{1}H-NMR of the complex **2** in DMSO-d_6 recorded on a 400 MHz Bruker NMR spectrometer.

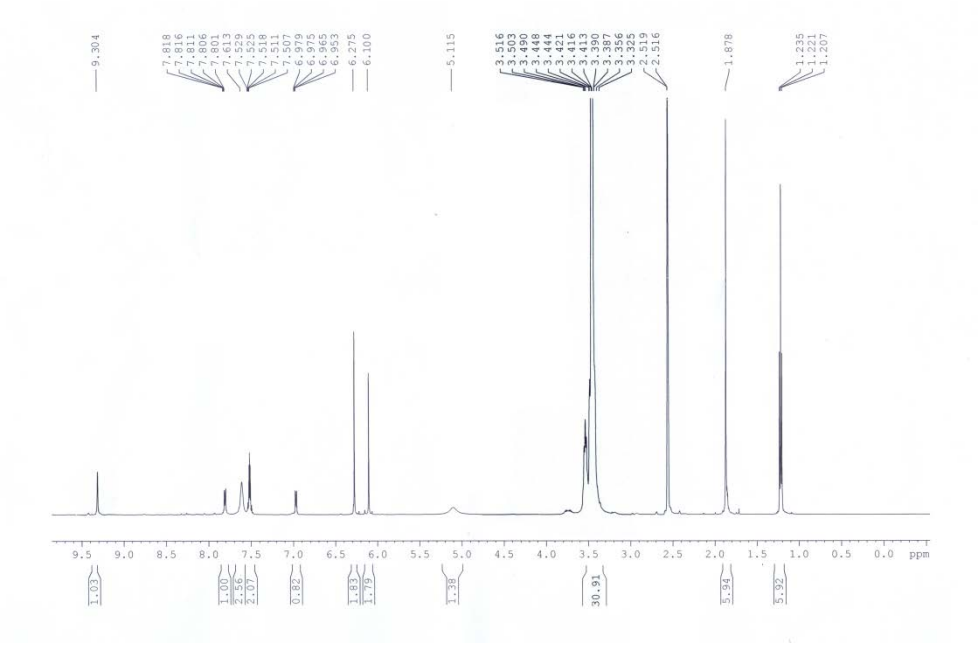

Figure S17. ^{1}H-NMR of the complex **3** in DMSO-d_6 recorded on a 400 MHz Bruker NMR spectrometer.

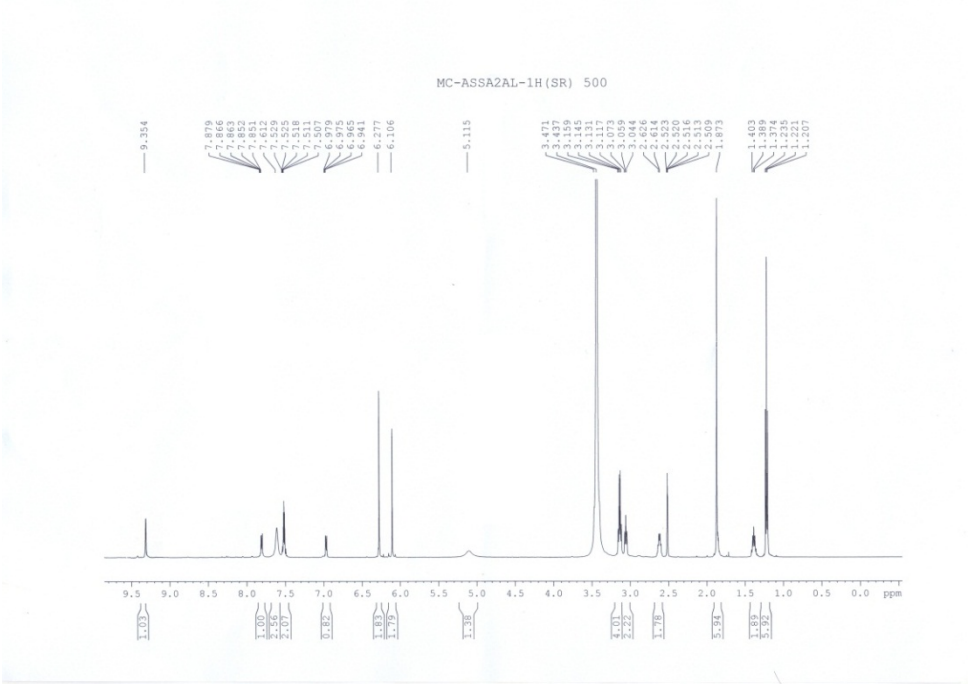

Figure S18. ^{1}H-NMR of the complex **4** in DMSO-d_6 recorded on a 400 MHz Bruker NMR spectrometer.

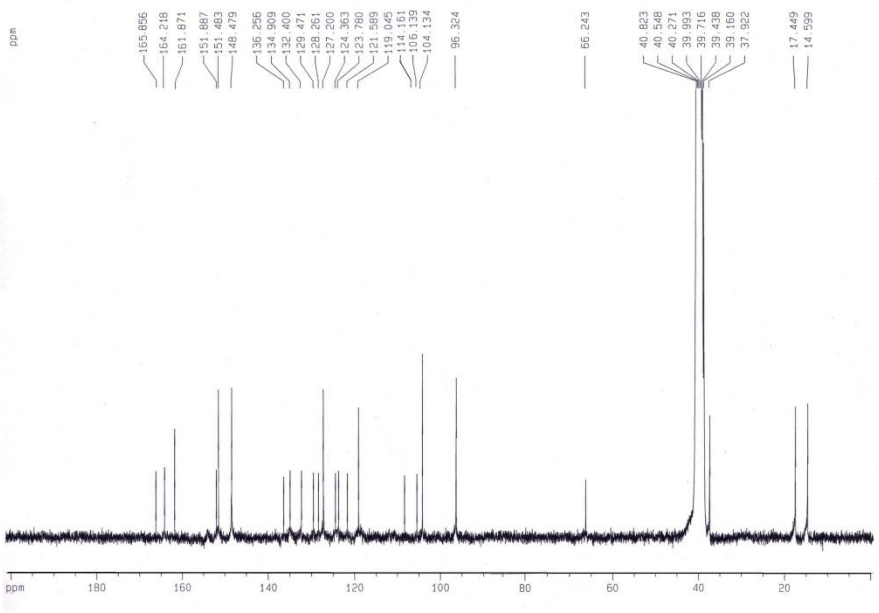

Figure S19. ^{13}C NMR spectrum of **H_3L1** in DMSO-d_6.

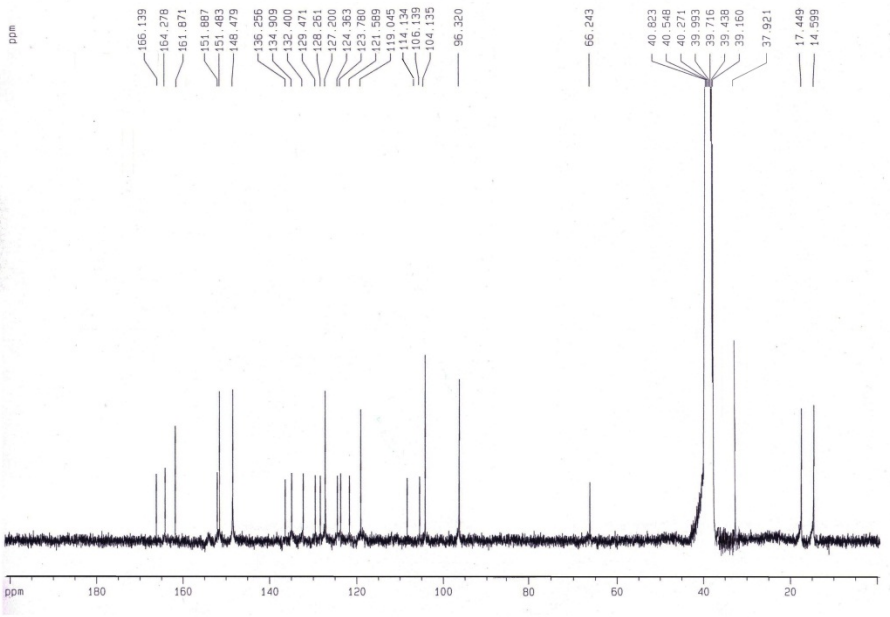

Figure S20. ^{13}C NMR spectrum of **H_3L2** in DMSO-d_6.

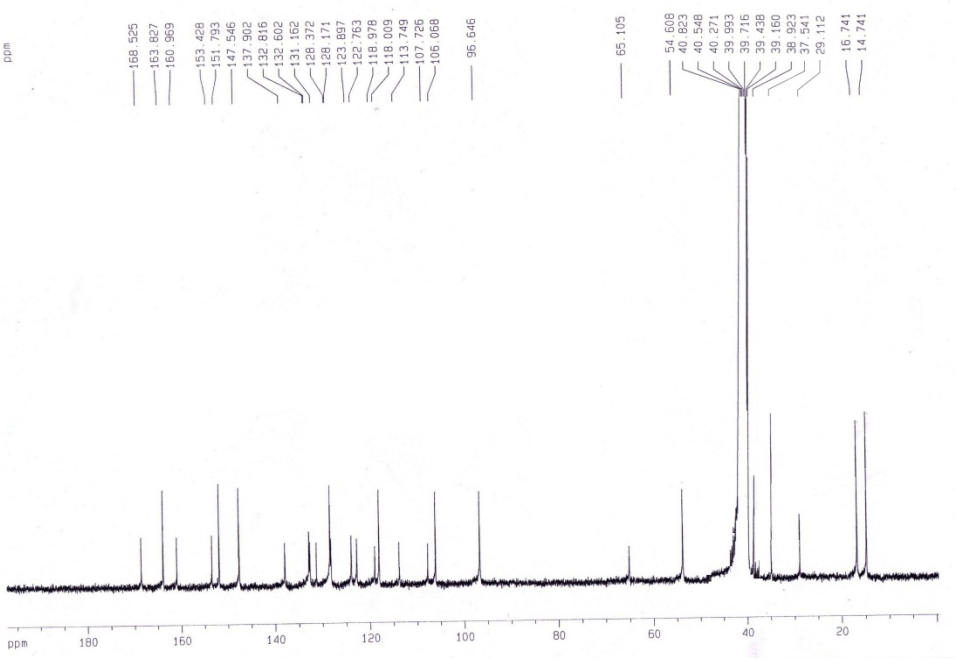

Figure S21. ^{13}C NMR spectrum of **H_3L3** in DMSO-d_6.

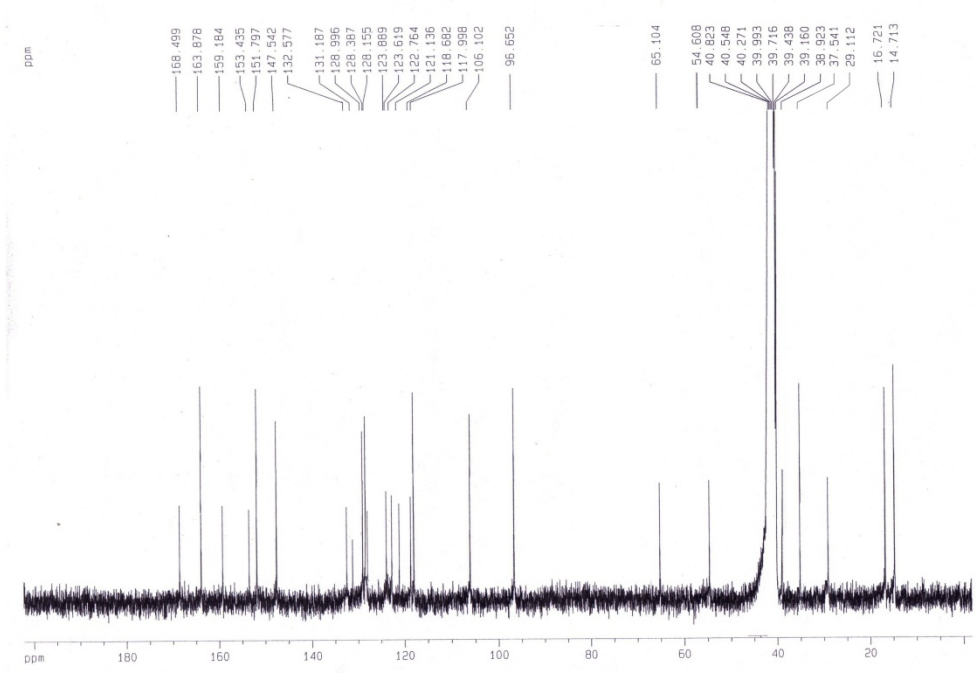

Figure S22. ^{13}C NMR spectrum of **H_3L4** in DMSO-d_6.

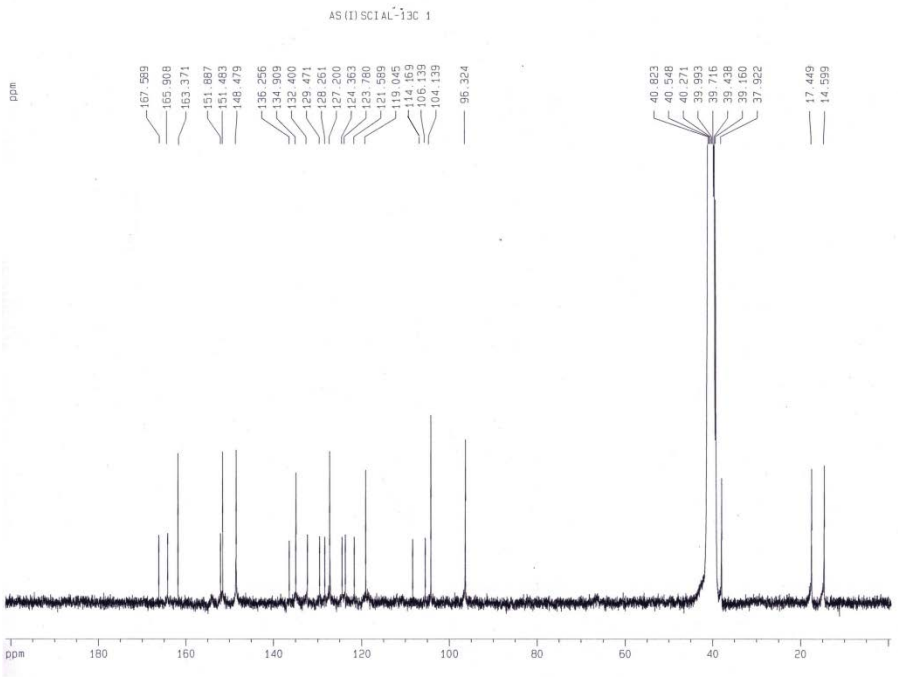

Figure S23. ^{13}C NMR spectrum of complex **1** in DMSO-d_6

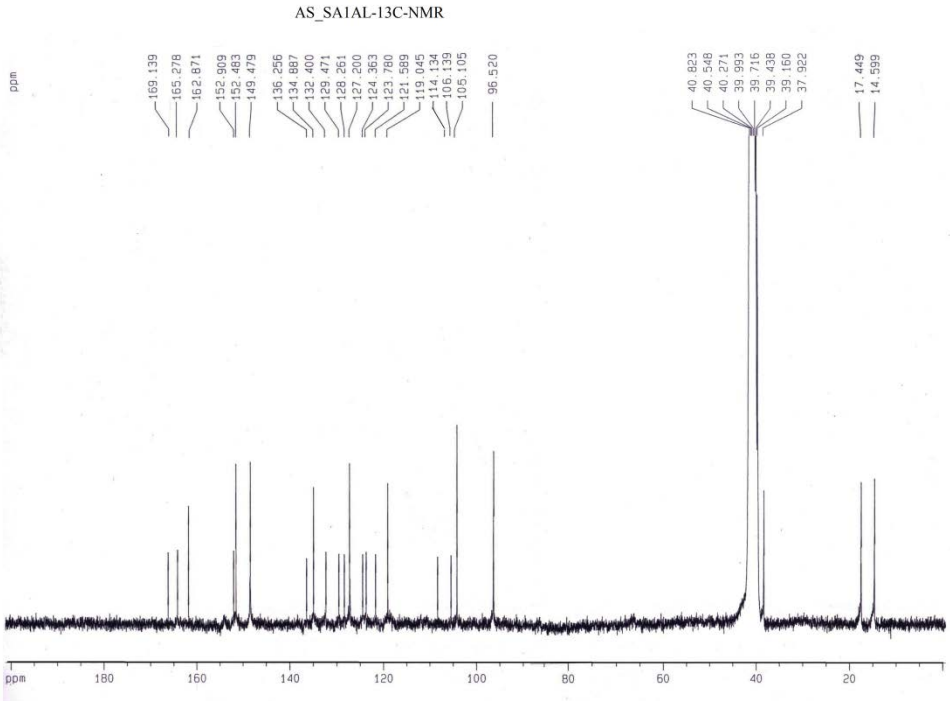

Figure S24. ^{13}C NMR spectrum of complex **2** in DMSO-d_6.

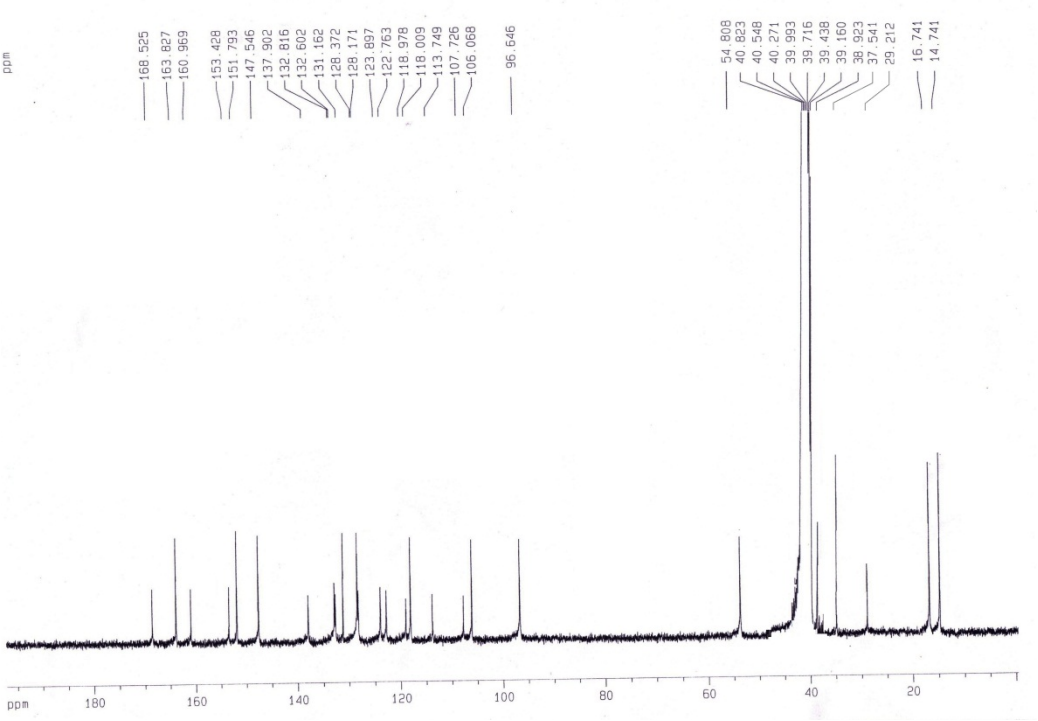

Figure S25. ^{13}C NMR spectrum of complex **3** in DMSO-d_6.

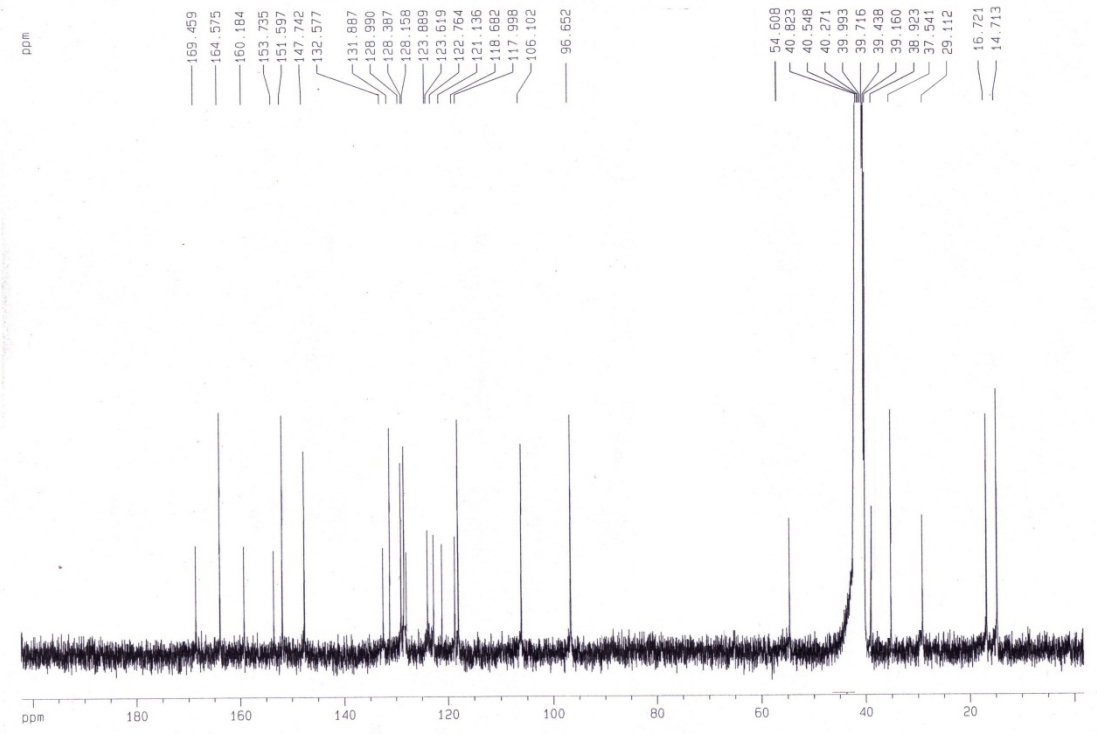

Figure S26. ^{13}C NMR spectrum of complex **4** in DMSO-d_6.

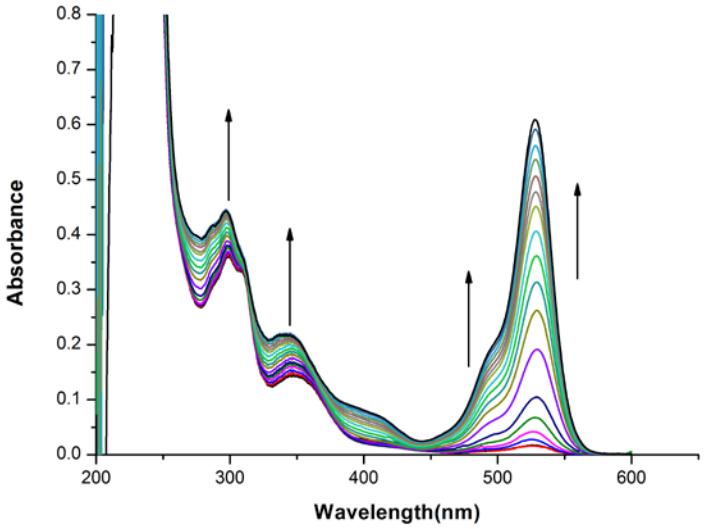

Figure S27. Absorption titration study of **H_3L2** (10 µM) with gradual addition of Al^{3+} ions, 0-11 µM in 10 mM HEPES buffer at pH 7.4.

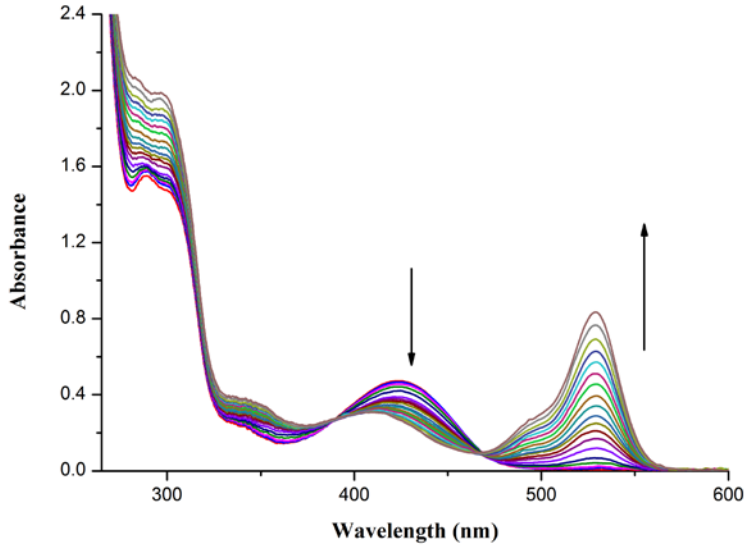

Figure S28. Absorption titration study of **H_3L3** (10 µM) with gradual addition of Al^{3+} ions, 0-11 µM in 10 mM HEPES buffer at pH 7.

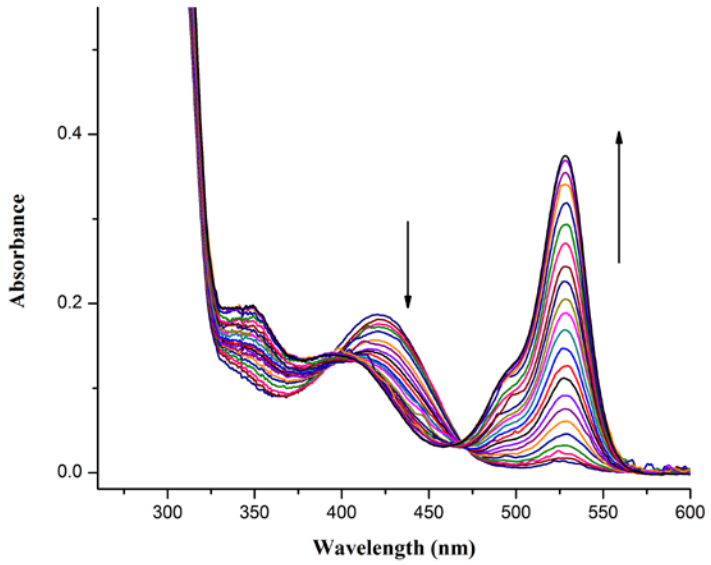

Figure S29. Absorption titration study of **H_3L4** (10 µM) with gradual addition of Al^{3+} ions, 0-11µM in 10 mM HEPES buffer at pH 7.4.

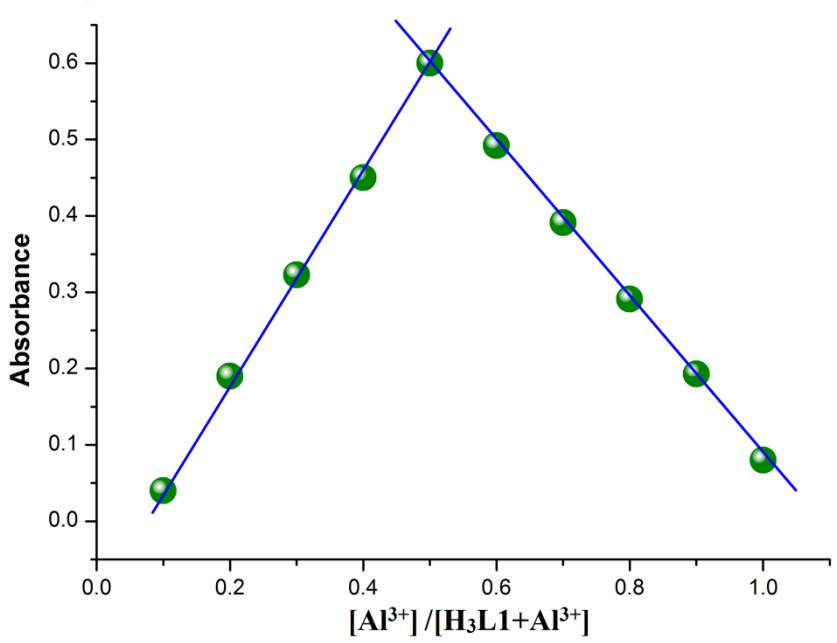

Figure S30. 1:1 binding stoichiometry has shown by Job's plot of complex**1**. Symbols and solid lines represent the experimental and simulated profiles, respectively.

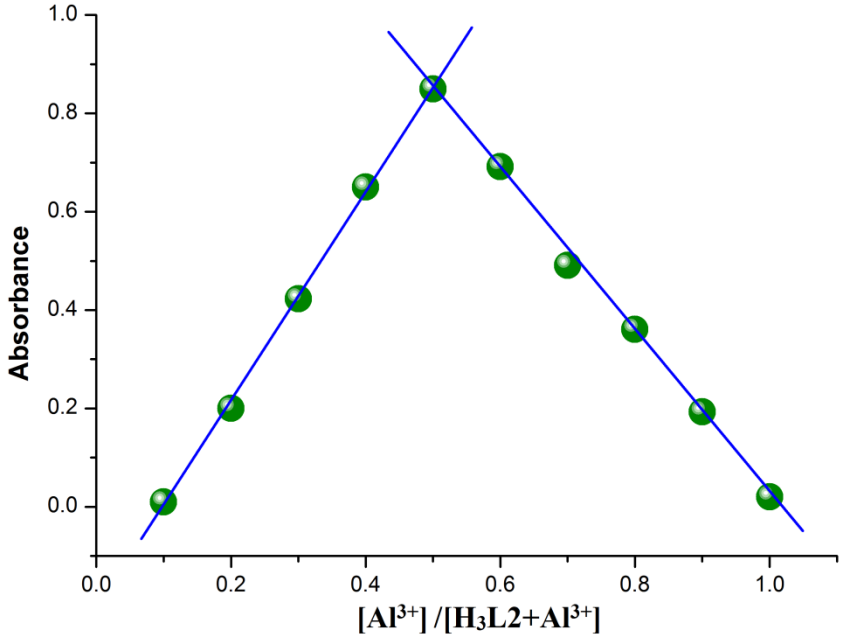

Figure S31. 1:1 binding stoichiometry has shown by Job's plot of complex **2**. Symbols and solid lines represent the experimental and simulated profiles, respectively.

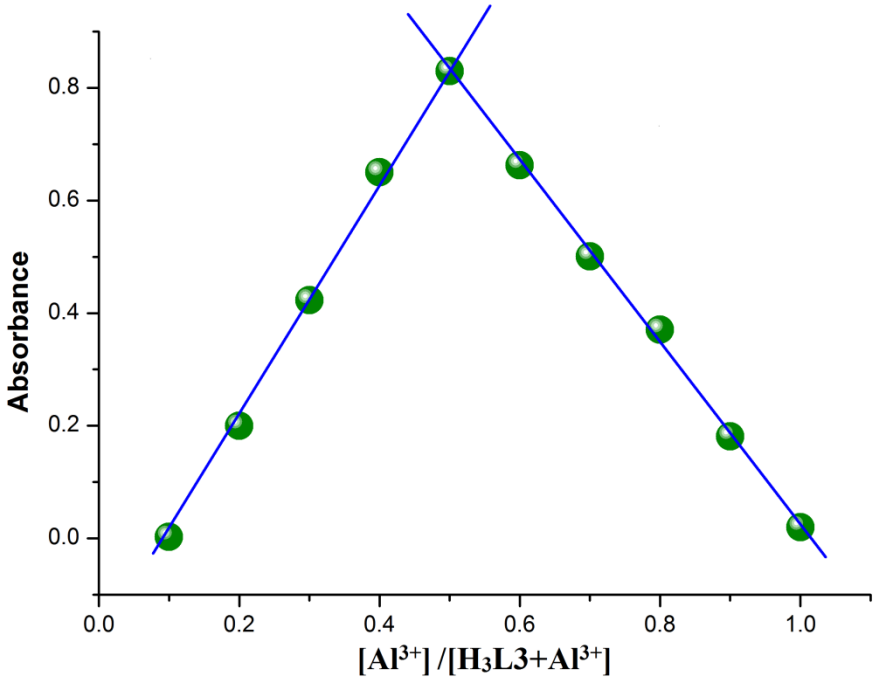

Figure S32. 1:1 binding stoichiometry has shown by Job's plot of complex **3**. Symbols and solid lines represent the experimental and simulated profiles, respectively.

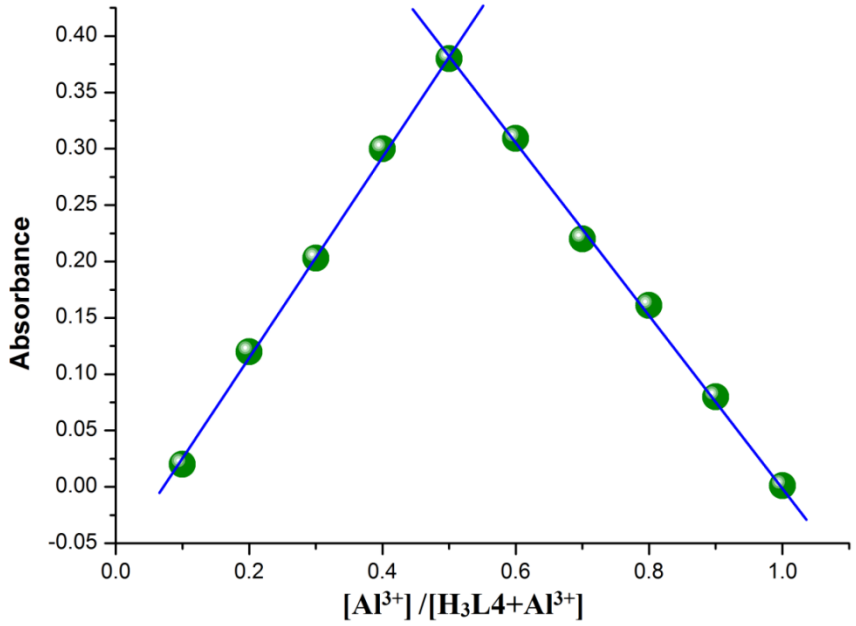

Figure S33. 1:1 binding stoichiometry has shown by Job's plot of complex **4**. Symbols and solid lines represent the experimental and simulated profiles, respectively.

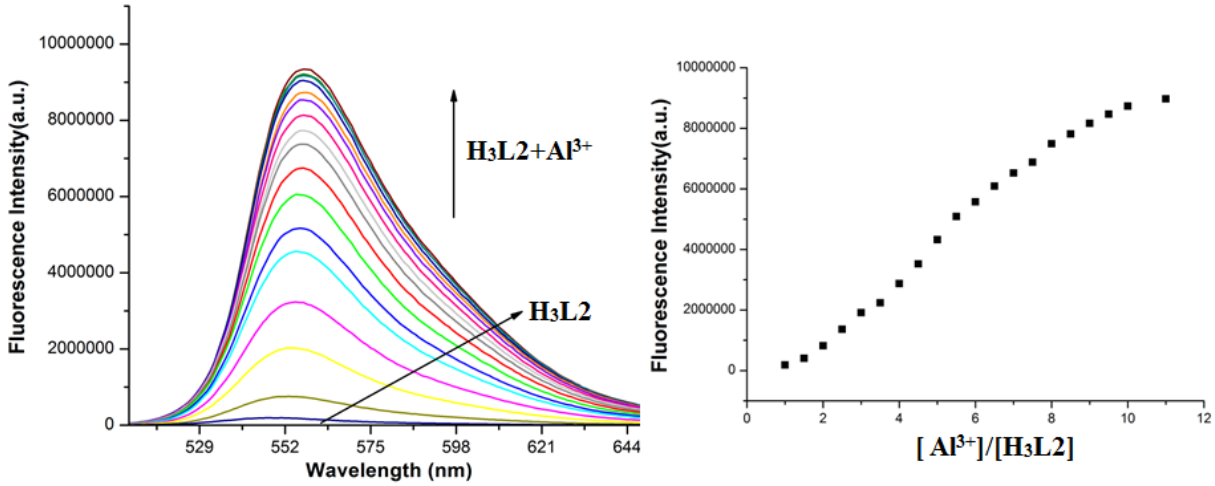

Figure S34. Fluorescence titration of **H_3L2** (10 μM) in 10 mM HEPES buffer at pH =7.4 by successive addition of Al^{3+} (0–11 μM) with λem= 555 nm (1/1 slit).

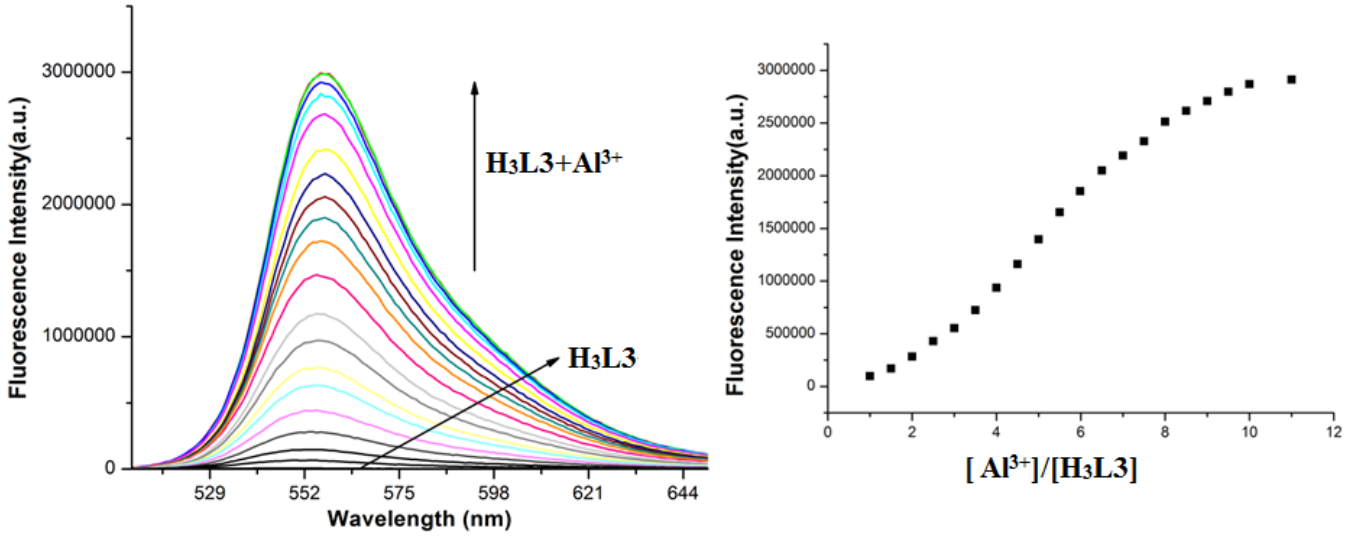

Figure S35. Fluorescence titration of **H_3L3** (10 μM) in 10 mM HEPES buffer at pH =7.4 by successive addition of Al^{3+} (0–11 μM) with λem= 555 nm (1/1 slit).

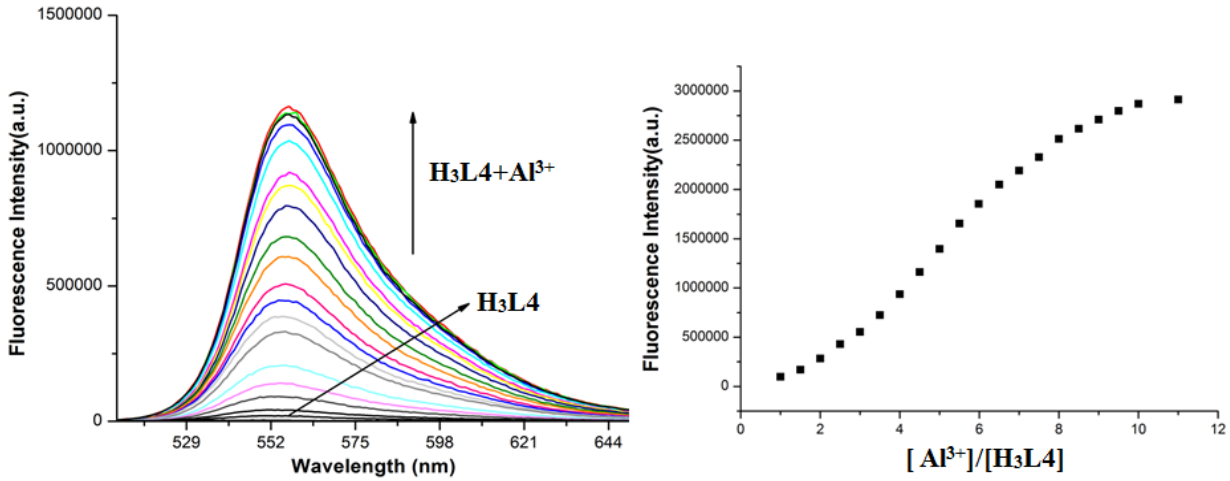

Figure S36. Fluorescence titration of **H_3L4** (10 μM) in 10 mM HEPES buffer at pH =7.4 by successive addition of Al^{3+} (0–11 μM) with λem= 555 nm (1/1 slit).

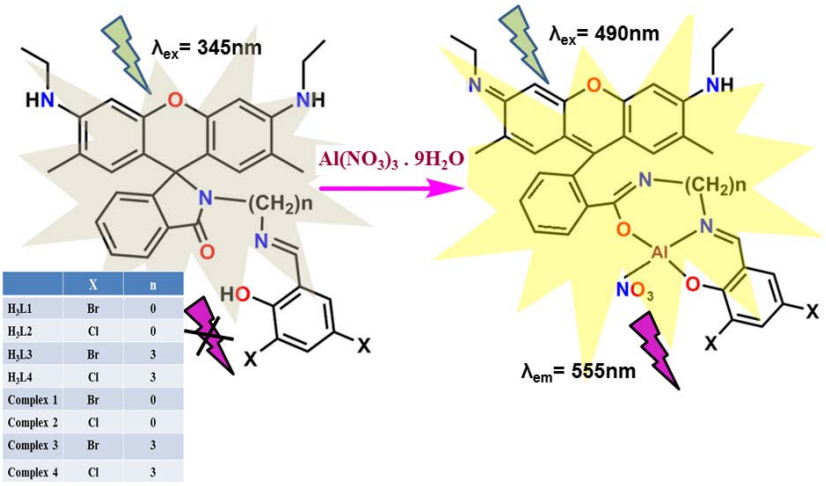

	X	n
H_3L1	Br	0
H_3L2	Cl	0
H_3L3	Br	3
H_3L4	Cl	3
Complex 1	Br	0
Complex 2	Cl	0
Complex 3	Br	3
Complex 4	Cl	3

Figure S37. Pictorial representation of spirolactam ring opening in presence of Al^{3+}ions.

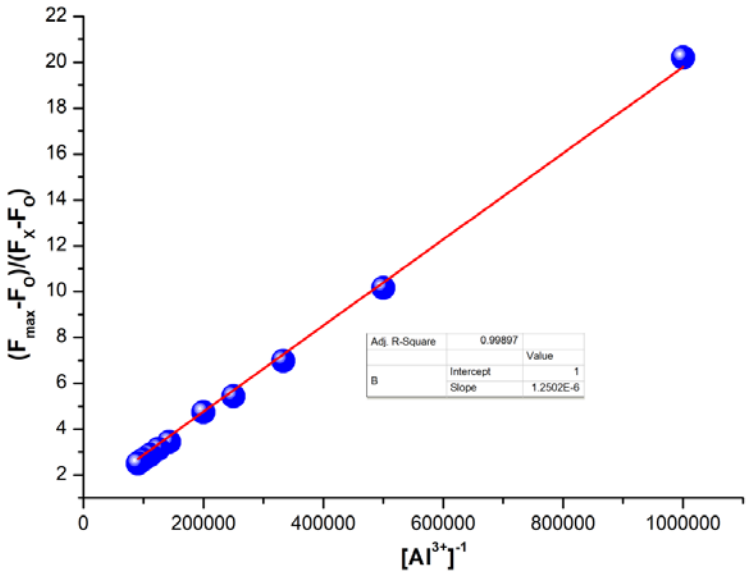

Figure S38. Benesi-Hildebrand plot for complex **1**. The plot is obtained after adding 10 μM Al^{3+} solution to the **H_3L1** solution (10 μM) (in 10 mM HEPES buffer medium, pH 7.4).

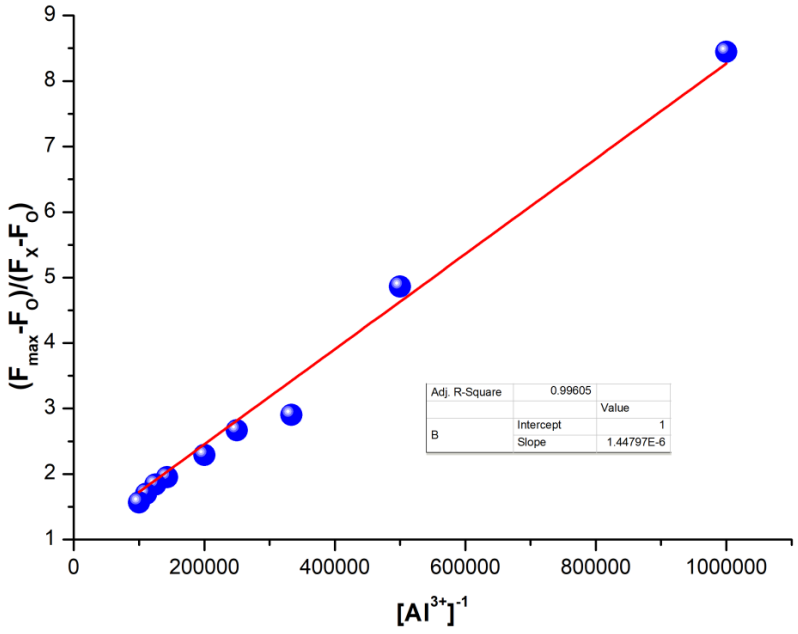

Figure S39. Benesi-Hildebrand plot for complex **2**. The plot is obtained after adding 10 μM Al^{3+} solution to the **H_3L2** solution (10 μM) (in 10 mM HEPES buffer medium, pH 7.4).

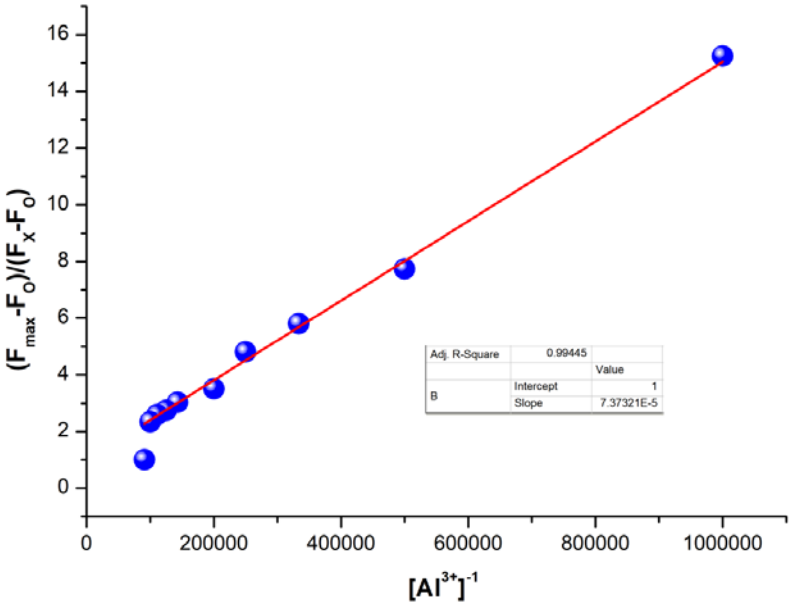

Figure S40. Benesi-Hildebrand plot for complex **3**. The plot is obtained after adding 10 μM Al^{3+} solution to the **H_3L3** solution (10 μM) (in 10 mM HEPES buffer medium, pH 7.4).

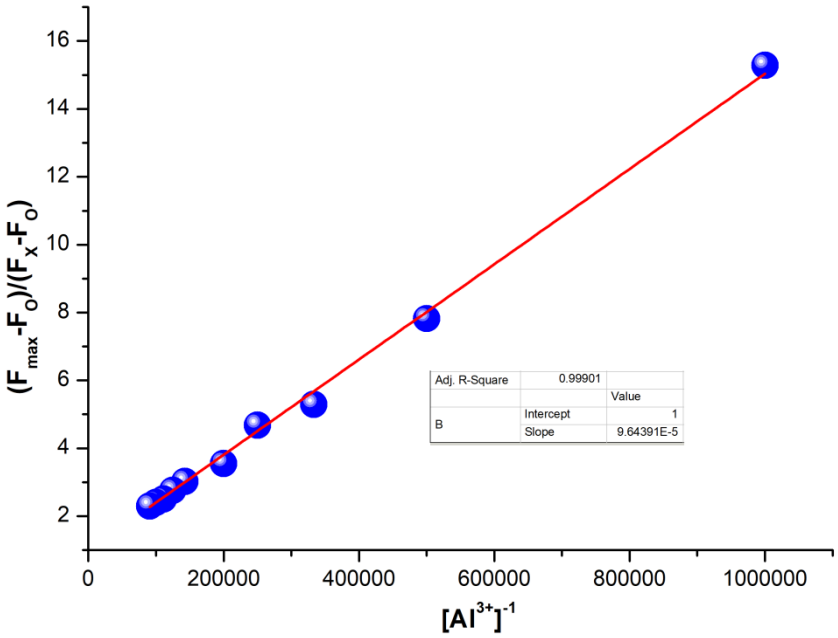

Figure S41. Benesi-Hildebrand plot for complex **4**. The plot is obtained after adding 10 μM Al^{3+} solution to the **H_3L4** solution (10 μM) (in 10 mM HEPES buffer medium, pH 7.4).

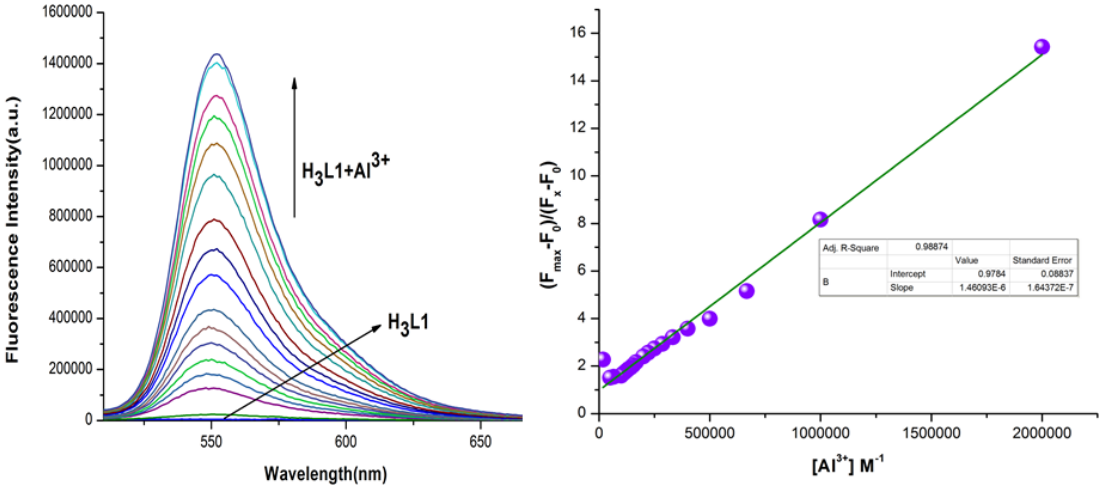

Figure S42. Fluorescence titration of **H_3L1** (10 μM) in THF solvent by gradual addition of Al^{3+} (0–11 μM) with λex= 490 nm and corresponding Benesi-Hildebrand plot.

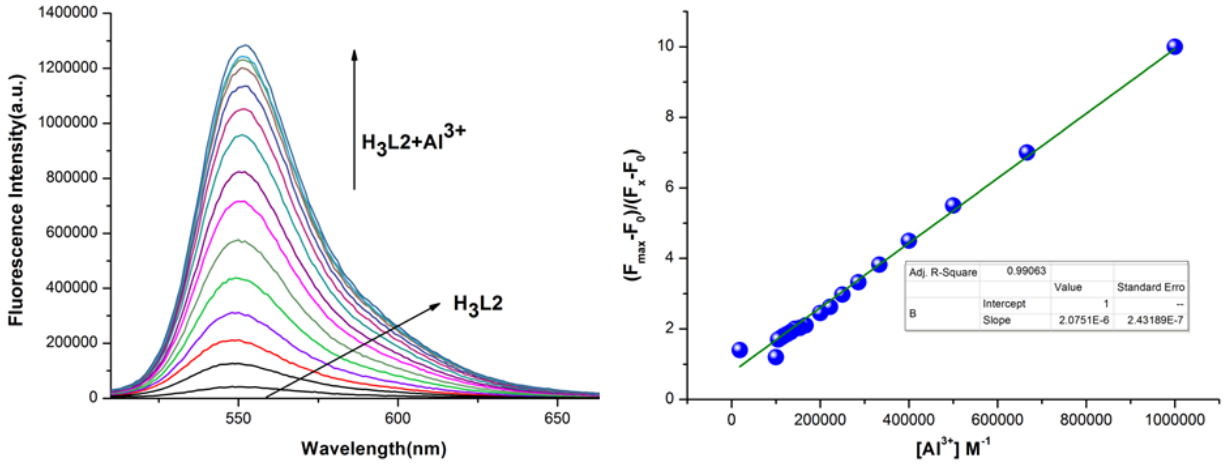

Figure S43. Fluorescence titration of **H_3L2** (10 µM) in THF solvent by gradual addition of Al^{3+} (0–11 µM) with λex= 490 nm and corresponding Benesi-Hildebrand plot.

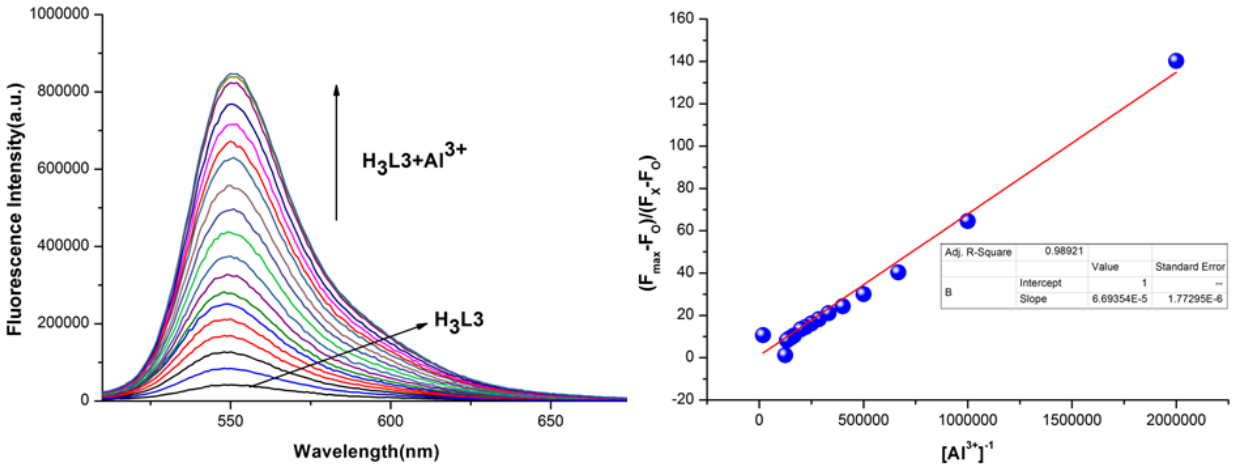

Figure S44. Fluorescence titration of **H_3L3** (10 µM) in THF solvent by gradual addition of Al^{3+} (0–11 µM) with λex= 490 nm and corresponding Benesi-Hildebrand plot.

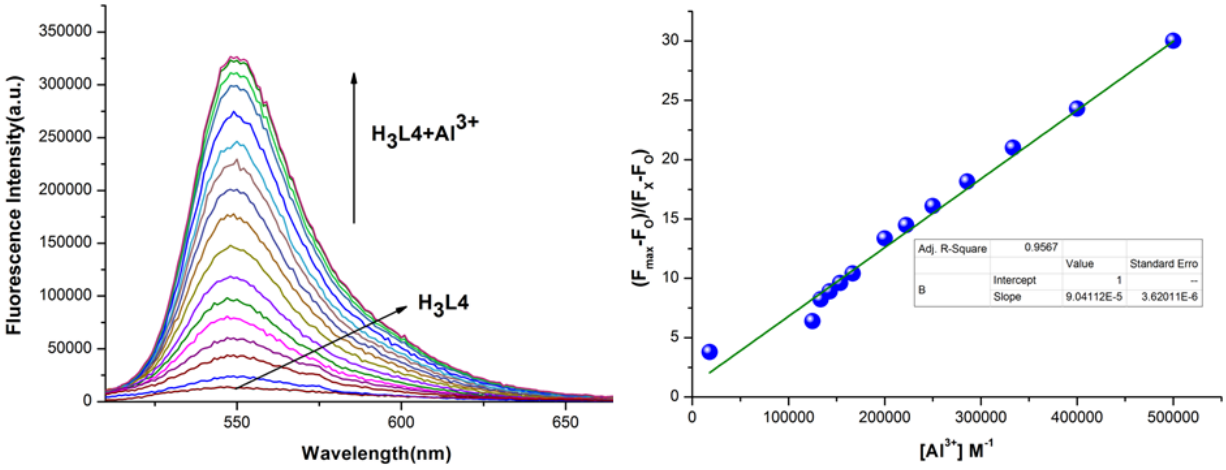

Figure S45. Fluorescence titration of **H_3L4** (10 μM) in THF solvent by gradual addition of Al^{3+} (0–11 μM) with λex= 490 nm and corresponding Benesi-Hildebrand plot.

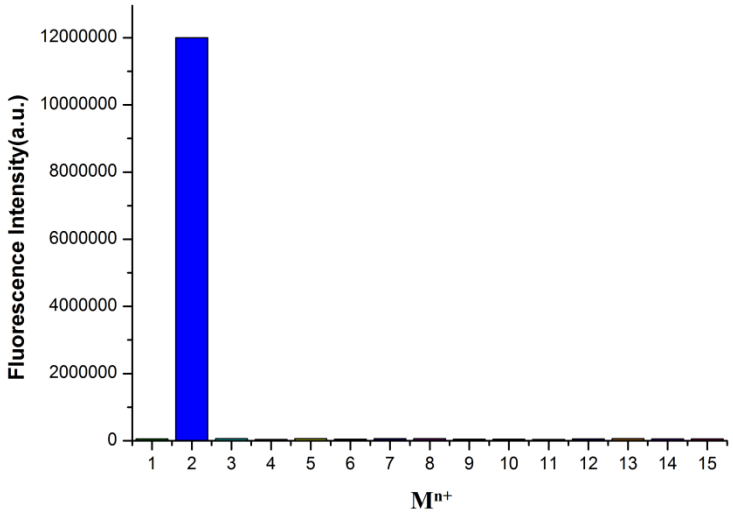

Figure S46. Relative fluorescence intensity diagram of chemosensor **H_3L1** in the presence of different cations in HEPES buffer at pH 7.4. 1=only **H_3L1** (10 μM); **H_3L1** (10 μM) + M^{n+}(10 μM), where M^{n+}=(2–Al^{3+}, 3–Cu^{2+}, 4–Cr^{3+}, 5–Fe^{3+}, 6–Hg^{2+}, 7–K^{+}, 8–Mn^{2+}, 9–Na^{+}, 10-Ni^{2+}, 11–Mg^{2+}, 12–Pb^{2+}, 13–Ca^{2+}, 14-Fe^{2+}, 15–Cd^{2+}).

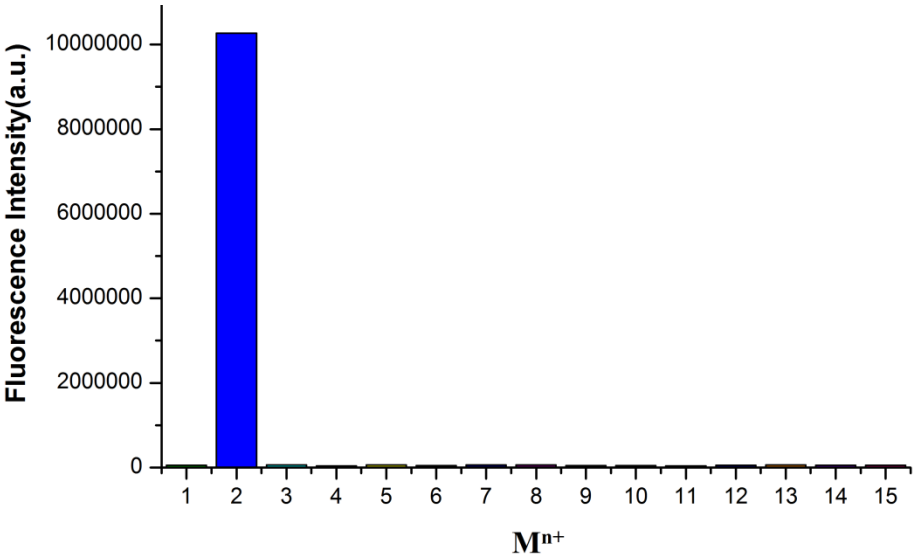

Figure S47. Relative fluorescence intensity diagram of chemosensor **H_3L2** in the presence of different cations in HEPES buffer at pH 7.4. 1=only **H_3L2** (10 μM); **H_3L2** (10 μM) + M^{n+}(10 μM), where M^{n+}=(2–Al^{3+}, 3–Cu^{2+}, 4–Cr^{3+}, 5–Fe^{3+}, 6–Hg^{2+}, 7–K^{+}, 8–Mn^{2+}, 9–Na^{+}, 10-Ni^{2+}, 11–Mg^{2+}, 12–Pb^{2+}, 13–Ca^{2+}, 14-Fe^{2+}, 15–Cd^{2+}).

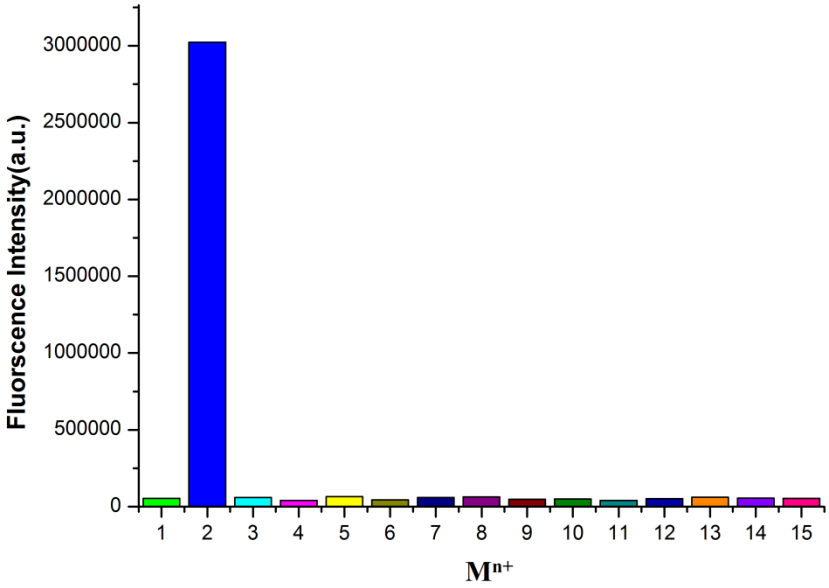

Figure S48. Relative fluorescence intensity diagram of chemosensor **H_3L3** in the presence of different cations in HEPES buffer at pH 7.4. 1=only **H_3L3** (10 μM); **H_3L3** (10 μM) + M^{n+}(10 μM), where M^{n+}=(2–Al^{3+}, 3–Cu^{2+}, 4–Cr^{3+}, 5–Fe^{3+}, 6–Hg^{2+}, 7–K^{+}, 8–Mn^{2+}, 9–Na^{+}, 10-Ni^{2+}, 11–Mg^{2+}, 12–Pb^{2+}, 13–Ca^{2+}, 14-Fe^{2+}, 15–Cd^{2+}).

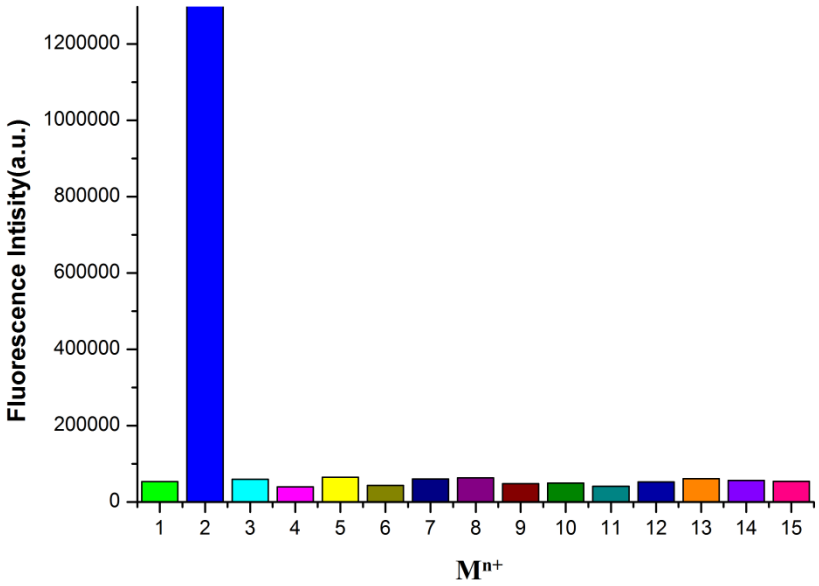

Figure S49. Relative fluorescence intensity diagram of chemosensor **H_3L4** in the presence of different cations in HEPES buffer at pH 7.4. 1=only **H_3L4** (10 µM); **H_3L4** (10 µM) + M^{n+}(10 µM), where M^{n+}=(2–Al^{3+}, 3–Cu^{2+}, 4–Cr^{3+}, 5–Fe^{3+}, 6–Hg^{2+}, 7–K^{+}, 8–Mn^{2+}, 9–Na^{+}, 10-Ni^{2+}, 11–Mg^{2+}, 12–Pb^{2+}, 13–Ca^{2+}, 14-Fe^{2+}, 15–Cd^{2+}).

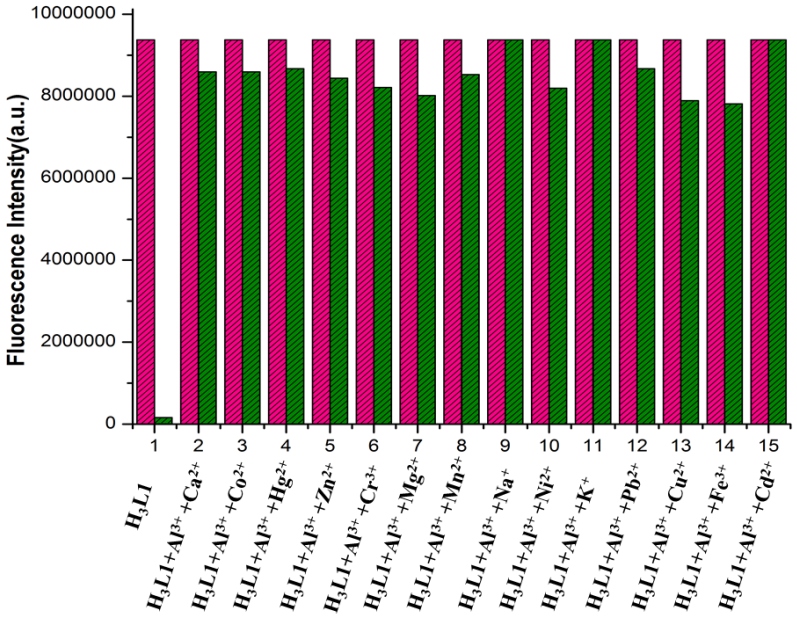

Figure S50. Relative fluorescence intensity diagram of [**H_3L2**-Al^{3+}] system in the presence of different cations in 10 mM HEPES buffer at pH 7.4. 1=only **H_3L2** and (2-15)= **H_3L2** (10 µM) + Al^{3+}(10 µM) + M^{n+}(40µM), where M^{n+}=(2–Ca^{2+}, 3–Co^{2+}, 4–Hg^{2+}, 5–Zn^{2+}, 6–Cr^{3+}, 7–Mg^{2+}, 8–Mn^{2+}, 9–Na^{+}, 10-Ni^{2+}, 11–K^{+}, 12–Pb^{2+}, 13–Cu^{2+}, 14- Fe^{3+}, 15–Cd^{2+}).

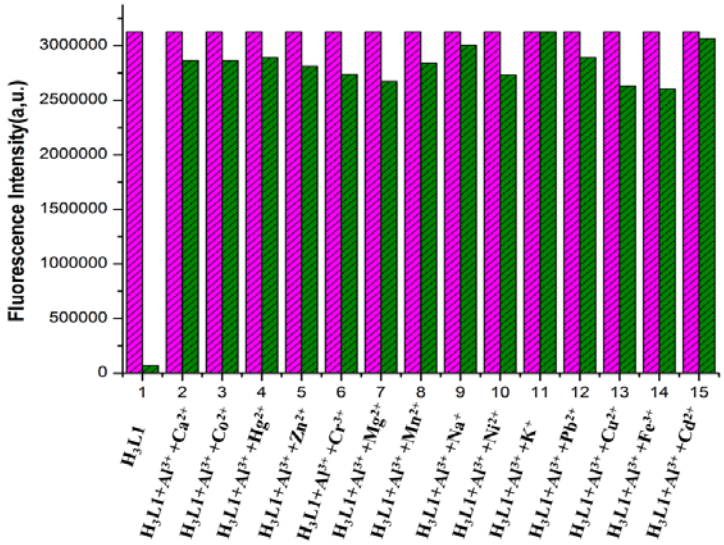

Figure S51. Relative fluorescence intensity diagram of [**H_3L3**-Al^{3+}] system in the presence of different cations in 10 mM HEPES buffer at pH 7.4. 1=only **H_3L3** and (2-15)= **H_3L3** (10 µM) + Al^{3+}(10 µM) + M^{n+}(40µM), where M^{n+}=(2–Ca^{2+}, 3–Co^{2+}, 4–Hg^{2+}, 5–Zn^{2+}, 6–Cr^{3+}, 7–Mg^{2+}, 8–Mn^{2+}, 9–Na^{+}, 10-Ni^{2+}, 11–K^{+}, 12–Pb^{2+}, 13–Cu^{2+}, 14- Fe^{3+}, 15–Cd^{2+}).

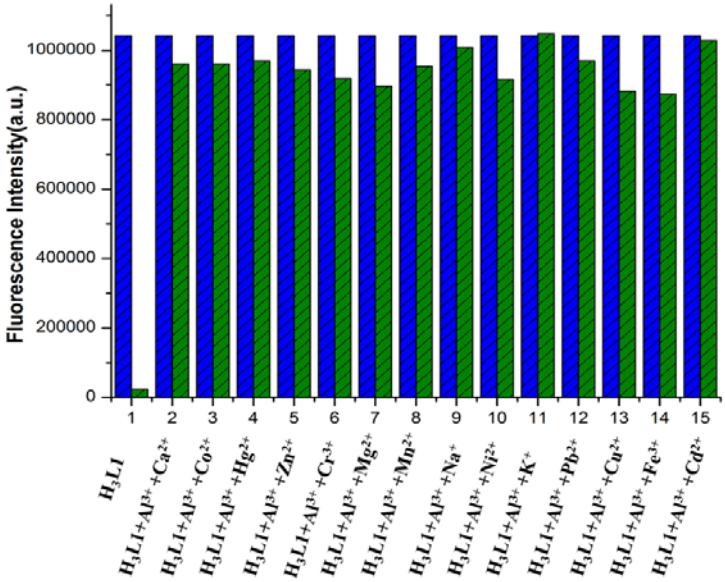

Figure S52. Relative fluorescence intensity diagram of [**H_3L4**-Al^{3+}] system in the presence of different cations in 10 mM HEPES buffer at pH 7.4. 1=only **H_3L4** and (2-15)= **H_3L4** (10 µM) + Al^{3+}(10 µM) + M^{n+}(40µM), where M^{n+}=(2–Ca^{2+}, 3–Co^{2+}, 4–Hg^{2+}, 5–Zn^{2+}, 6–Cr^{3+}, 7–Mg^{2+}, 8–Mn^{2+}, 9–Na^{+}, 10-Ni^{2+}, 11–K^{+}, 12–Pb^{2+}, 13–Cu^{2+}, 14- Fe^{3+}, 15–Cd^{2+}).

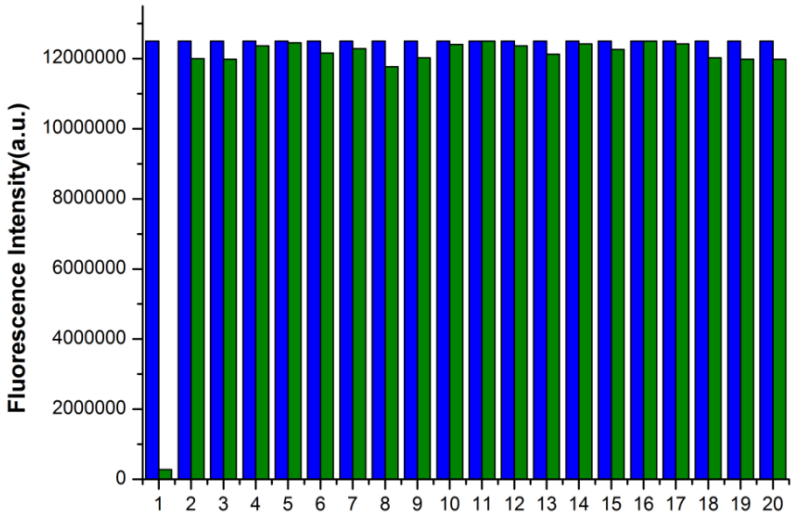

Figure S53. Relative fluorescence intensity diagram of [**H_3L1**-Al^{3+}] system in the presence of different anions in HEPES buffer medium (10 mM) at pH 7.4. 1=only **H_3L1** (10 µM) and (2-20)= **H_3L1** (10 µM) + Al^{3+}(10 µM) + Anions (40 µM), Anions = 2-$S_2O_3^{2-}$, 3-S^{2-}, 4-SO_3^{2-}, 5- HSO_4^-, 6-SO_4^{2-}, 7-SCN^-, 8-N_3^-, 9-OCN^-, 10-AsO_4^{3-},11-$H_2PO_4^-$, 12-HPO_4^{2-}, 13-PO_4^{3-}, 14-ClO_4^-, 15-AcO^-, 16-NO_3^-, 17-F^-, 18- Cl^-, 19-PF_6^-, 20-$P_2O_7^{4-}$.

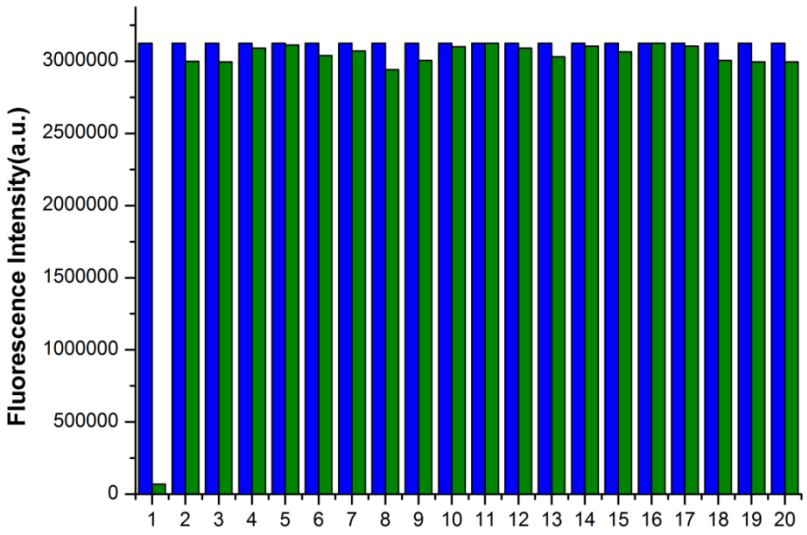

Figure S54. Relative fluorescence intensity diagram of [**H_3L2**-Al^{3+}] system in the presence of different anions in HEPES buffer medium (10 mM) at pH 7.4. 1=only **H_3L2** (10 µM) and (2-20)= **H_3L2** (10 µM) + Al^{3+}(10 µM) + Anions (40 µM), Anions = 2-$S_2O_3^{2-}$, 3-S^{2-}, 4-SO_3^{2-}, 5-HSO_4^-, 6- SO_4^{2-}, 7-SCN^-, 8-N_3^-, 9-OCN^-, 10-AsO_4^{3-},11-$H_2PO_4^-$, 12-HPO_4^{2-}, 13-PO_4^{3-}, 14-ClO_4^-, 15-AcO^-, 16-NO_3^-, 17-F^-, 18- Cl^-, 19-PF_6^-, 20-$P_2O_7^{4-}$

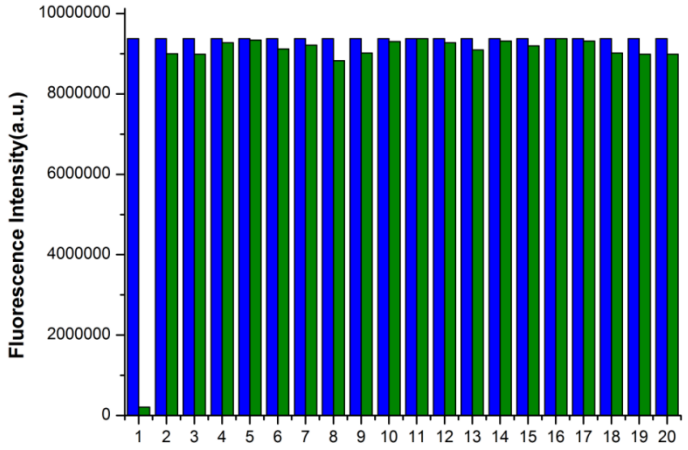

Figure S55. Relative fluorescence intensity diagram of [**H_3L3**-Al^{3+}] system in the presence of different anions in HEPES buffer medium (10 mM) at pH 7.4. 1=only **H_3L3** (10 µM) and (2-20)= **H_3L3** (10 µM) + Al^{3+}(10 µM) + Anions (40 µM), Anions = 2-$S_2O_3^{2-}$, 3-S^{2-}, 4-SO_3^{2-}, 5-HSO_4^-, 6- SO_4^{2-}, 7-SCN^-, 8-N_3^-, 9-OCN^-, 10-AsO_4^{3-},11-$H_2PO_4^-$, 12-HPO_4^{2-}, 13-PO_4^{3-}, 14-ClO_4^-, 15-AcO^-, 16-NO_3^-, 17-F^-, 18- Cl^-, 19-PF_6^-, 20-$P_2O_7^{4-}$.

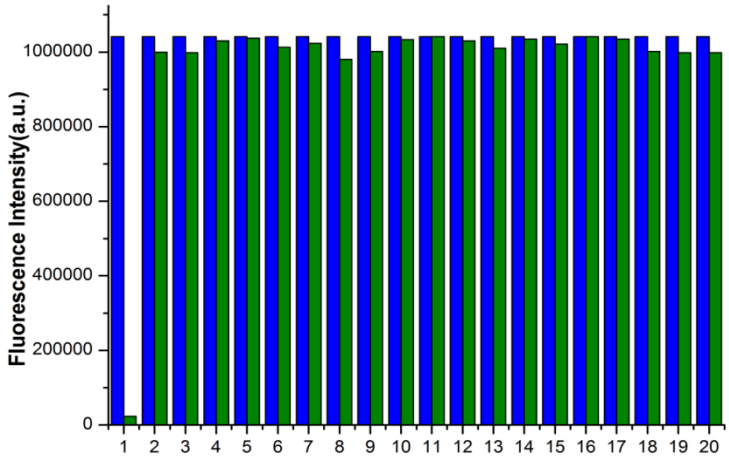

Figure S56. Relative fluorescence intensity diagram of [**H_3L4**-Al^{3+}] system in the presence of different anions in HEPES buffer medium (10 mM) at pH 7.4. 1=only **H_3L4** (10 µM) and (2-20)= **H_3L4** (10 µM) + Al^{3+}(10 µM) + Anions (40 µM), Anions = 2-$S_2O_3^{2-}$, 3-S^{2-}, 4-SO_3^{2-}, 5-HSO_4^-, 6- SO_4^{2-}, 7-SCN^-, 8-N_3^-, 9-OCN^-, 10-AsO_4^{3-},11-$H_2PO_4^-$, 12-HPO_4^{2-}, 13-PO_4^{3-}, 14-ClO_4^-, 15-AcO^-, 16-NO_3^-, 17-F^-, 18- Cl^-, 19-PF_6^-, 20-$P_2O_7^{4-}$.

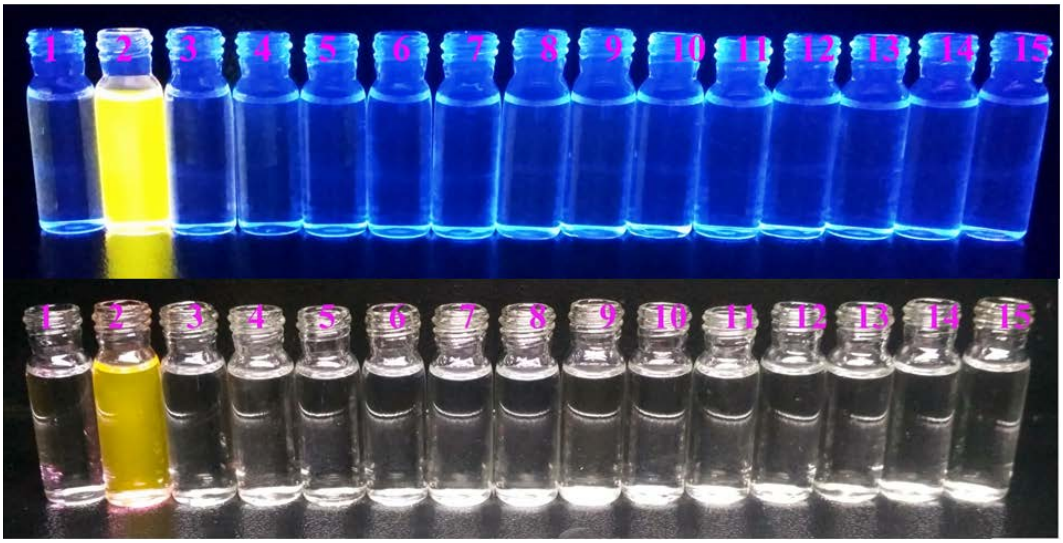

Figure S57. Visual colour changes of chemosensor **H_3L2** (10μM) in presence of common metal ions (1equivalent) in 10 mM HEPES buffer (pH 7.4). The images in below row and above row were taken under visible light and UV light respectively. Where 1= only **H_3L2,** 2-15= **H_3L2**+ different metal ions (Al^{3+}, Cu^{2+}, Cd^{2+},Pb^{2+}, Hg^{2+}, Mn^{2+}, Fe^{3+}, Co^{2+},Ni^{2+}, K^{+}, Na^{+}, Mg^{2+}, Ca^{2+} and Zn^{2+} respectively).

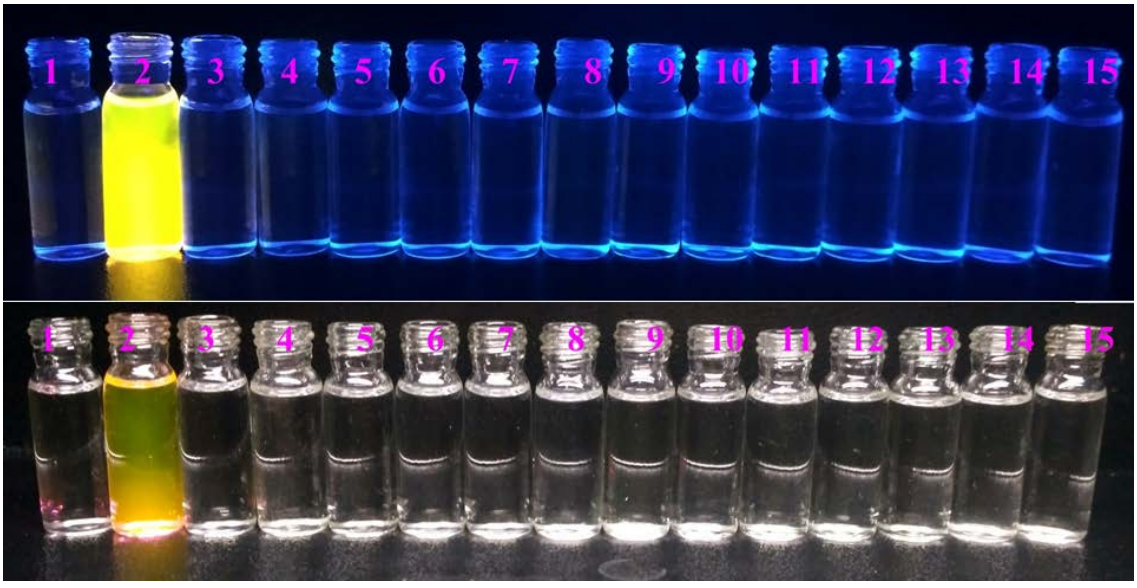

Figure S58. Visual colour changes of chemosensor **H_3L3** (10μM) in presence of common metal ions (1equivalent) in 10 mM HEPES buffer (pH 7.4). The images in below row and above row were taken under visible light and UV light respectively. Where 1= only **H_3L3,** 2-15= **H_3L3**+ different metal ions (Al^{3+}, Cu^{2+}, Cd^{2+},Pb^{2+}, Hg^{2+}, Mn^{2+}, Fe^{3+}, Co^{2+},Ni^{2+}, K^{+}, Na^{+}, Mg^{2+}, Ca^{2+} and Zn^{2+} respectively).

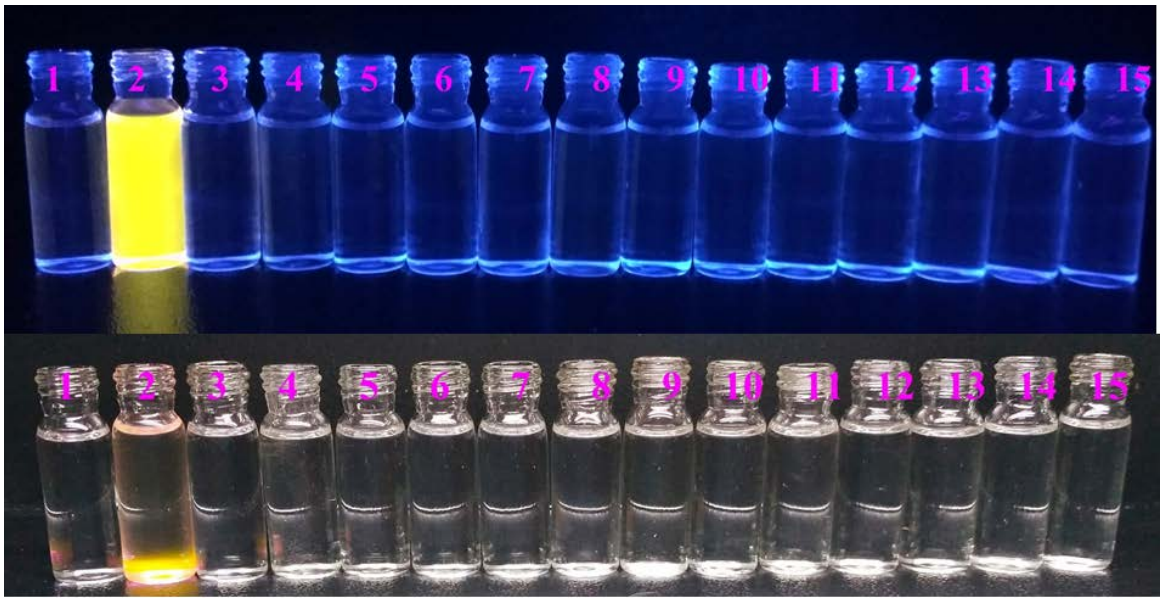

Figure S59. Visual colour changes of chemosensor **H_3L4** (10μM) in presence of common metal ions (1equivalent) in 10 mM HEPES buffer (pH 7.4). The images in below row and above row were taken under visible light and UV light respectively. Where 1= only **H_3L4,** 2-15= **H_3L4**+ different metal ions (Al^{3+}, Cu^{2+}, Cd^{2+},Pb^{2+}, Hg^{2+}, Mn^{2+}, Fe^{3+}, Co^{2+},Ni^{2+}, K^{+}, Na^{+}, Mg^{2+}, Ca^{2+} and Zn^{2+} respectively).

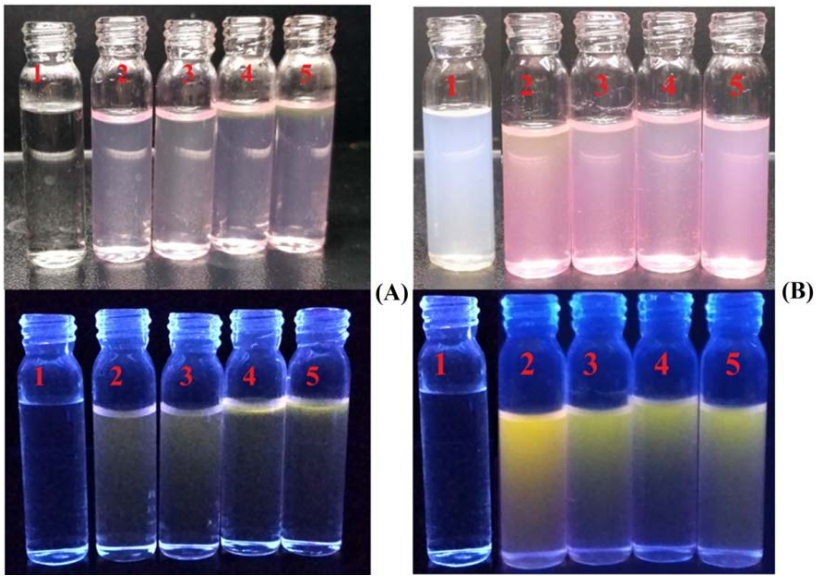

Figure S60. Visual colour changes of real samples under normal light (above) and UV lamp (below) in presence of chemosensors (**H_3L1- H_3L4**). (A) Laboratory tap water (1= Only laboratory tap water, 2-5=laboratory tap water + **H_3L1- H_3L4).** (B) Saloon waste water, (1= Only saloon waste water, 2-5= Saloon waste water + **H_3L1- H_3L4).**

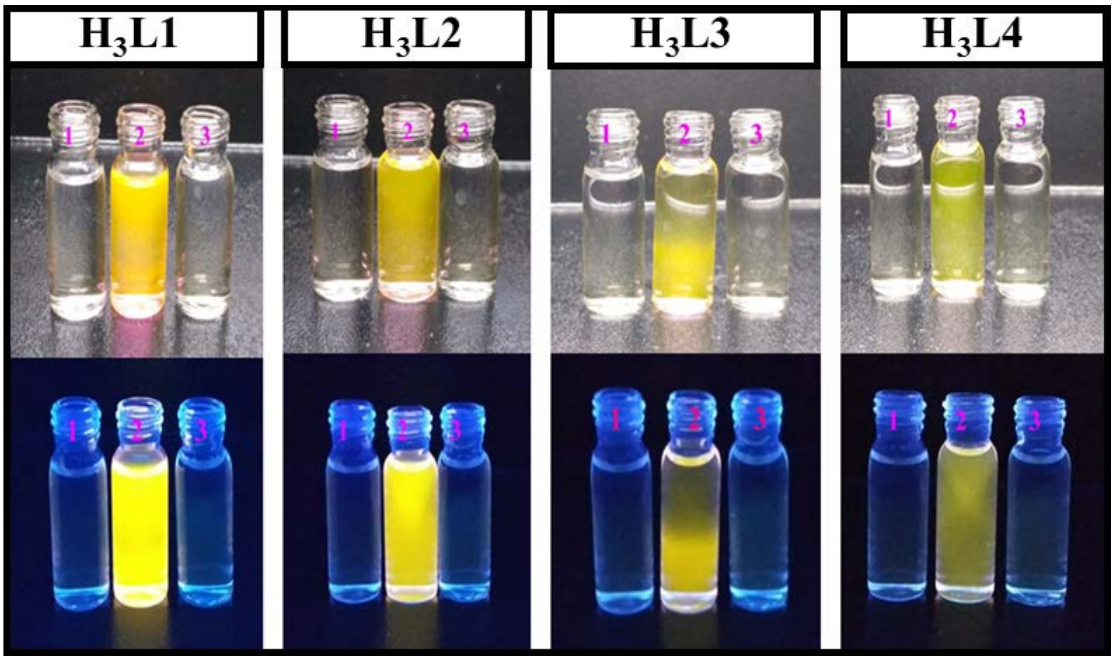

Figure S61. Visual colour changes in reversibility experiments. For **H_3L1-H_3L4**, 1= Only **H_3L1-H_3L4** (10μM), 2= **H_3L1-H_3L4** (10μM) + Al^{3+}(10μM), 3= **H_3L1-H_3L4** (10μM) + Al^{3+}(10μM) + $EDTA^{2-}$(10μM) under UV and normal light, respectively.

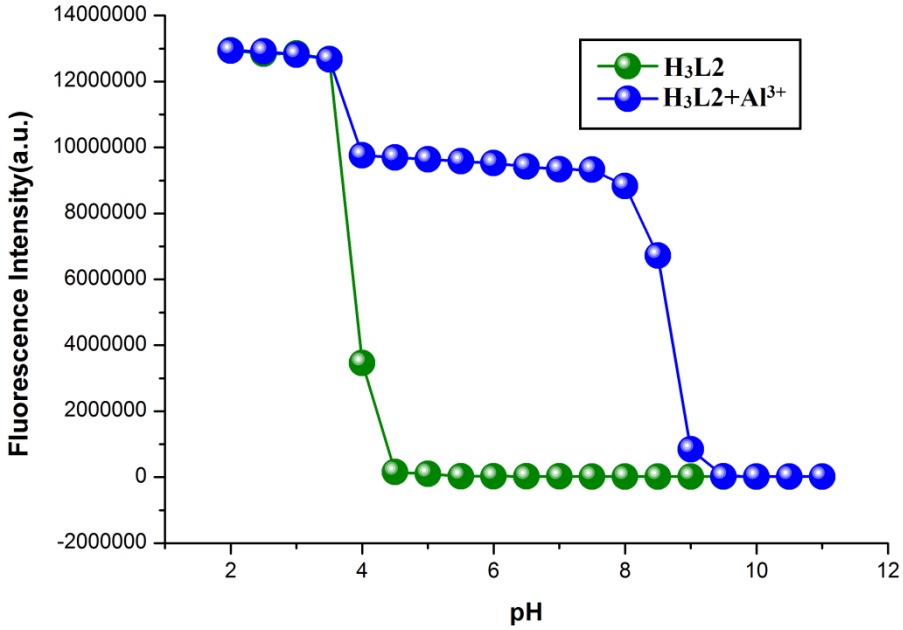

Figure S62. Fluorescence intensity of **H_3L2** (10 μM) in the absence and presence of Al^{3+} ions (10 μM) at various pH values in 10 mM HEPES buffer.

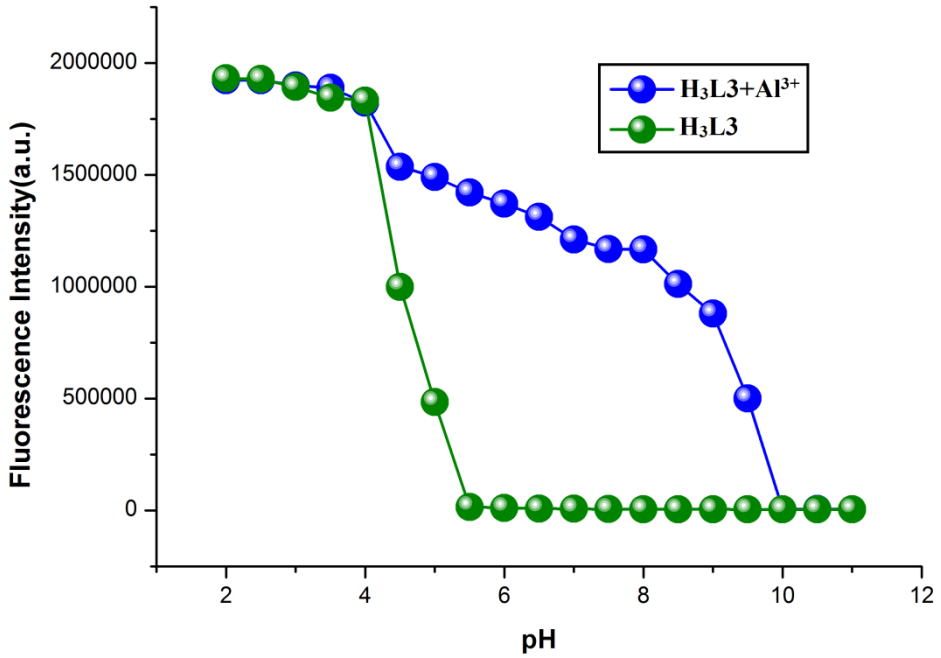

Figure S63. Fluorescence intensity of **H_3L3** (10 µM) in the absence and presence of Al^{3+} ions (10 µM) at various pH values in 10 mM HEPES buffer.

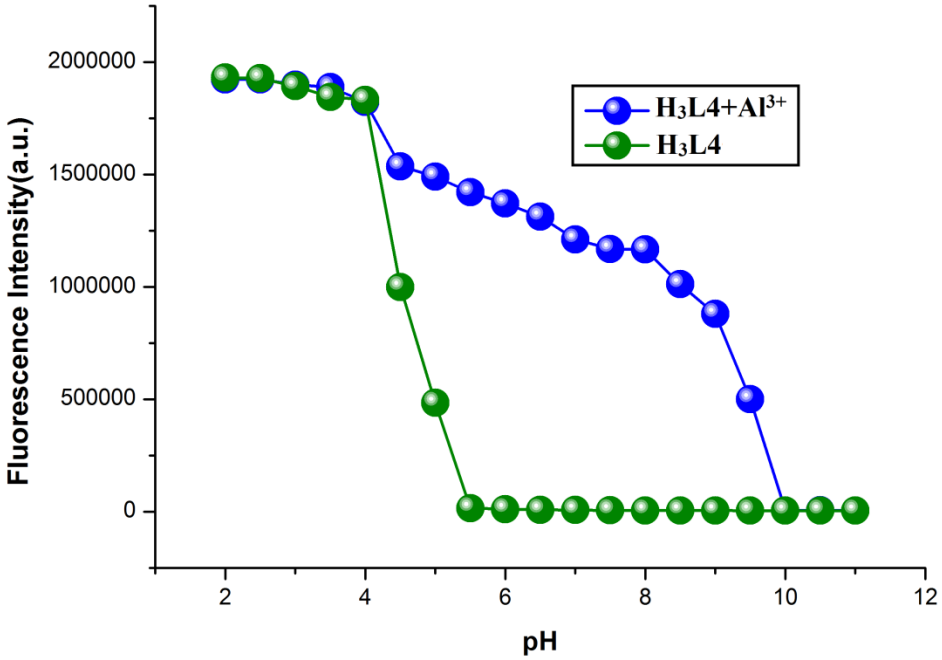

Figure S64. Fluorescence intensity of **H_3L4** (10 µM) in the absence and presence of Al^{3+} ions (10 µM) at various pH values in 10 mM HEPES buffer.

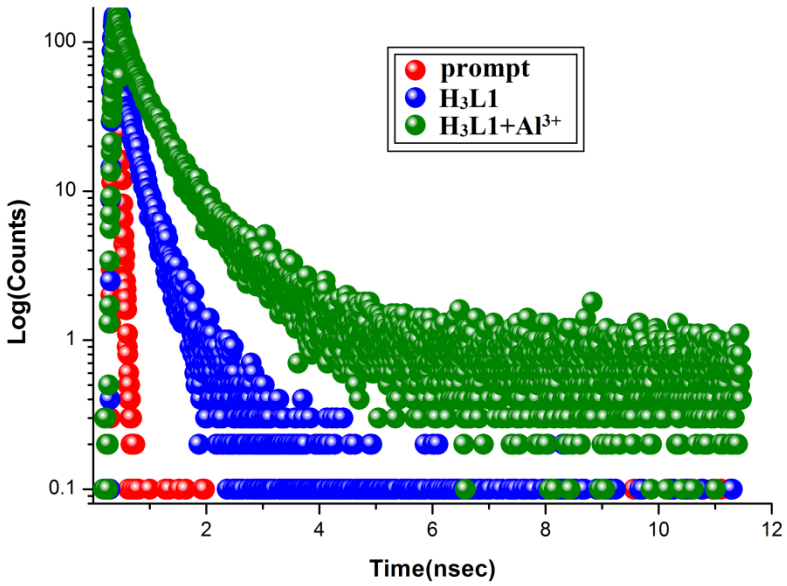

Figure S65. Time-resolved fluorescence decay curves (logarithm of normalized intensity vs time in ns) of **H_3L1** in the absence ( ) and presence ( ) of Al^{3+}ion, ( ) indicates decay curve for the scattered.

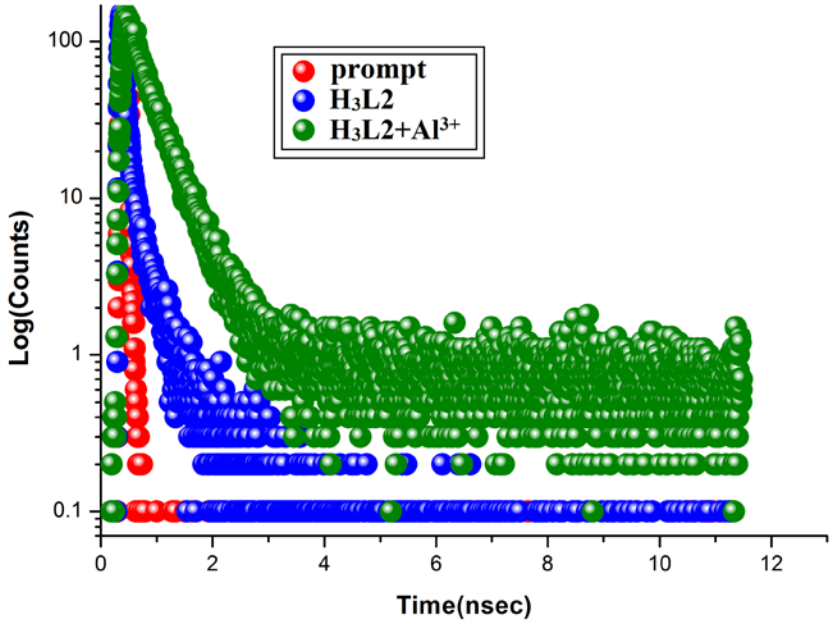

Figure S66. Time-resolved fluorescence decay curves (logarithm of normalized intensity vs time in ns) of **H_3L2** in the absence ( ) and presence ( ) of Al^{3+}ion, ( ) indicates decay curve for the scattered.

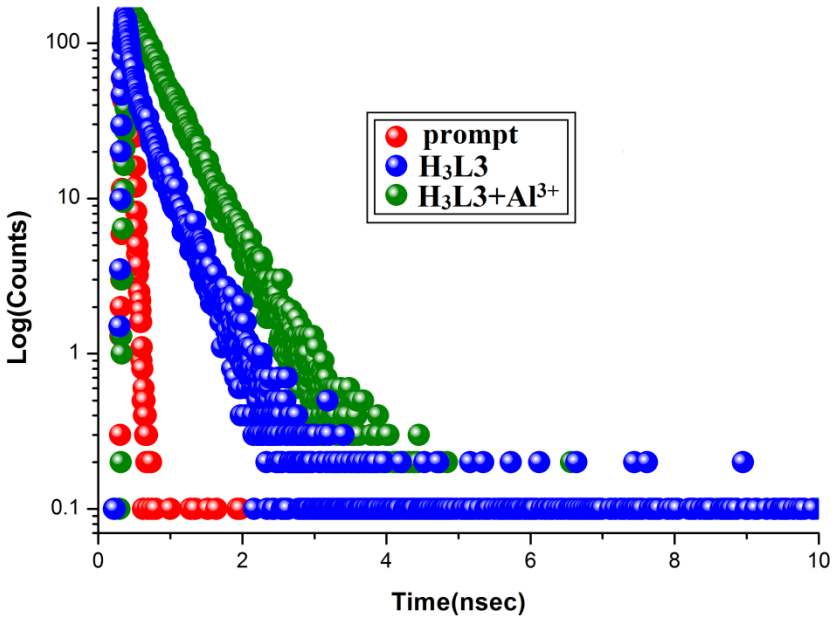

Figure S67. Time-resolved fluorescence decay curves (logarithm of normalized intensity vs time in ns) of **H_3L3** in the absence ( ) and presence ( ) of Al^{3+}ion, ( ) indicates decay curve for the scattered.

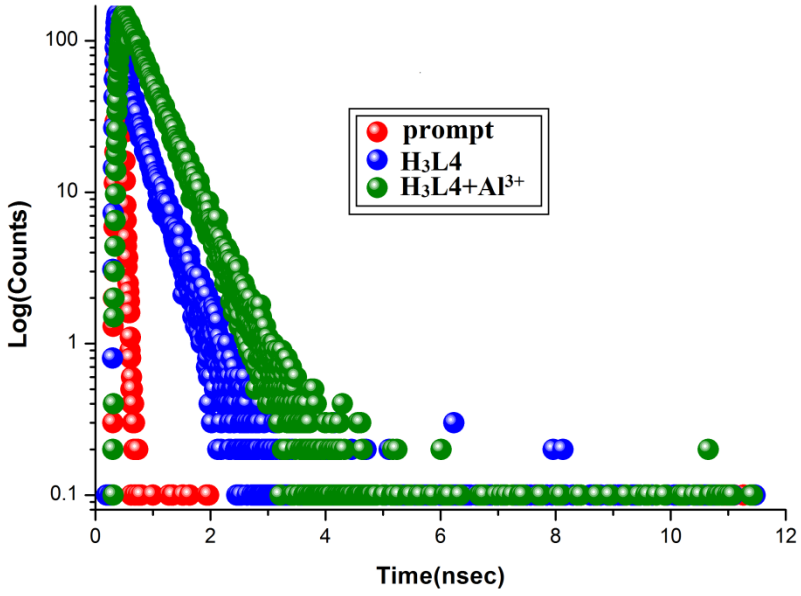

Figure S68. Time-resolved fluorescence decay curves (logarithm of normalized intensity vs time in ns) of **H_3L4** in the absence ( ) and presence ( ) of Al^{3+}ion, ( ) indicates decay curve for the scattered.

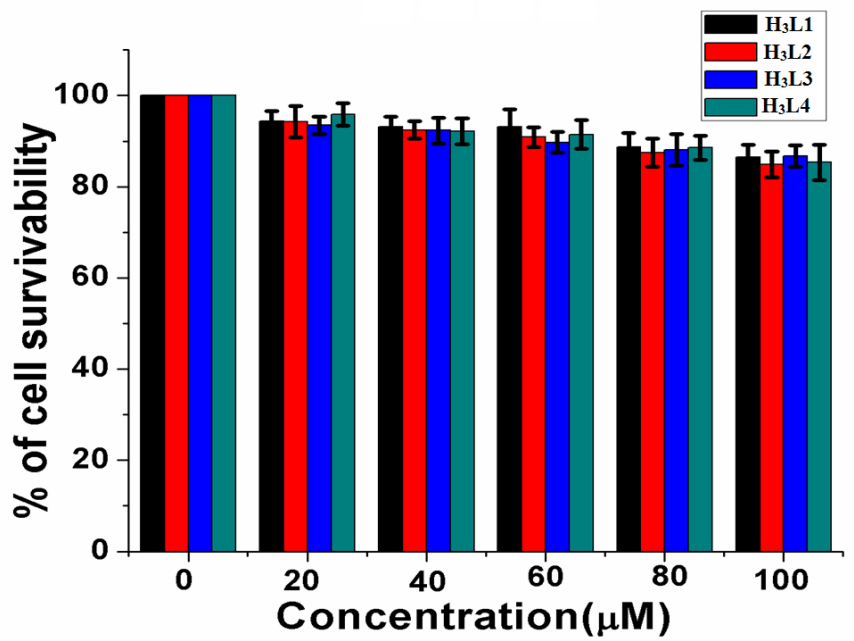

Figure S69. Survivability of WI38 cells exposed to **H_3L1-H_3L4.**

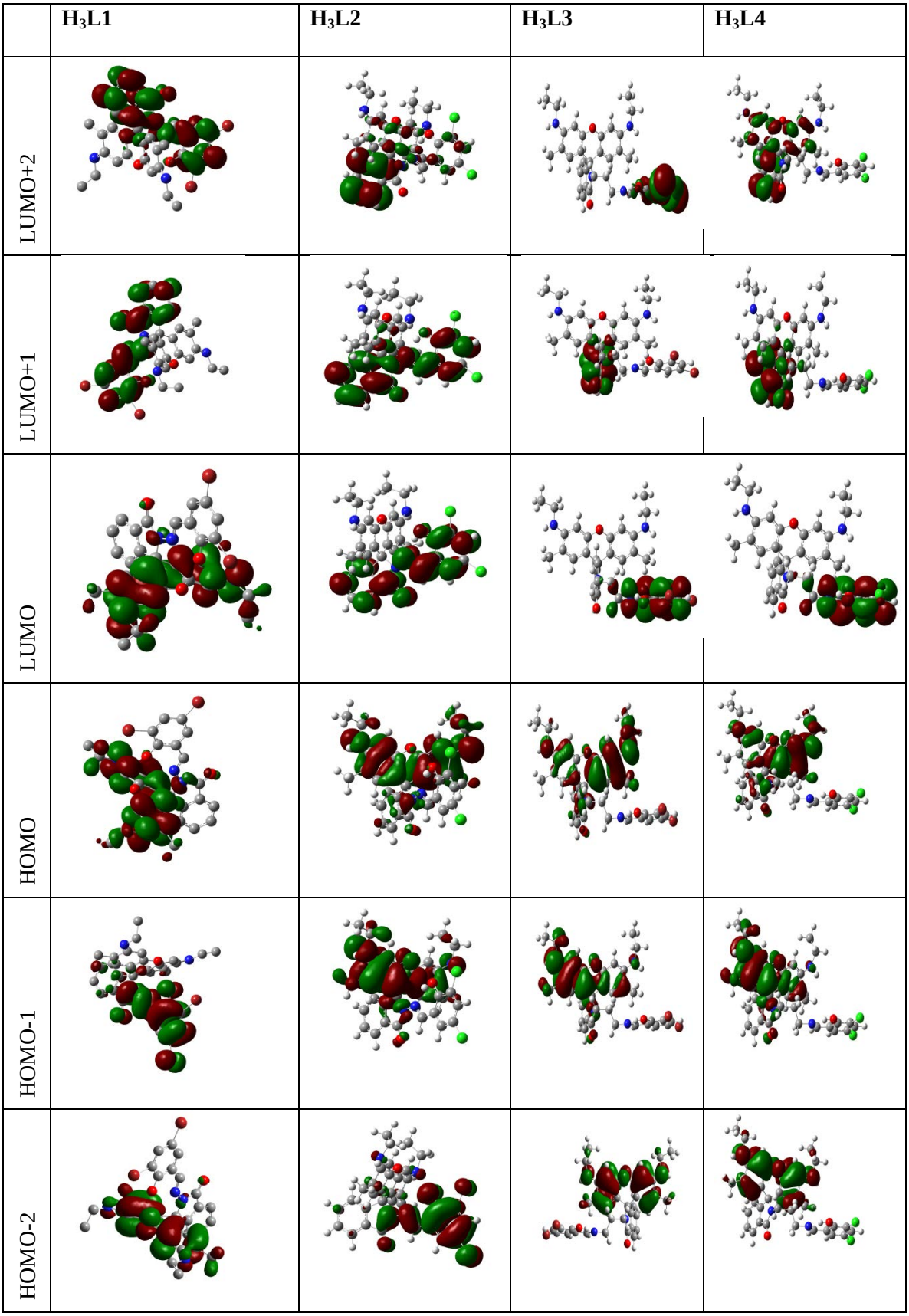

Figure S70. Selected contour plots of molecular orbitals of **H_3L1-H_3L4**.

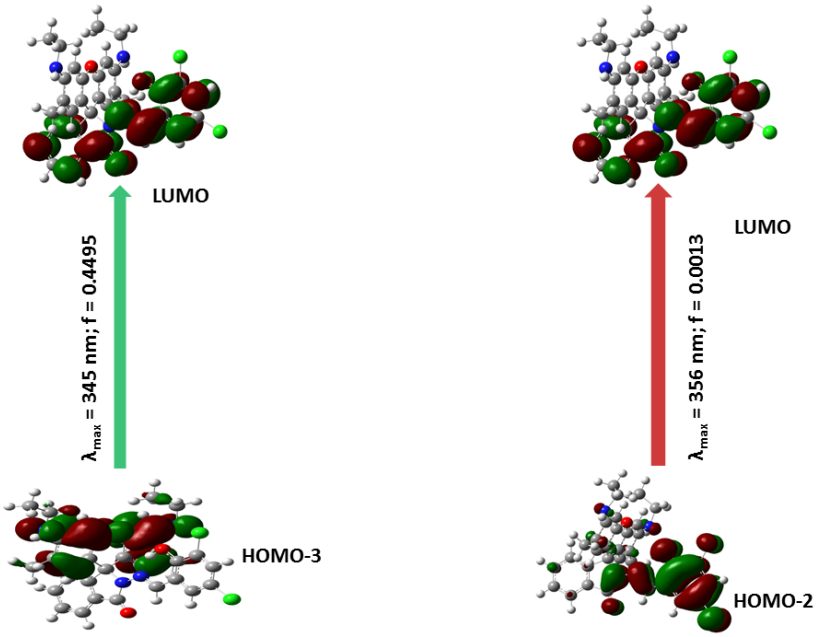

Figure S71. Pictorial representation of key transitions involved in UV-Vis absorption of chemosensor **H_3L2**.

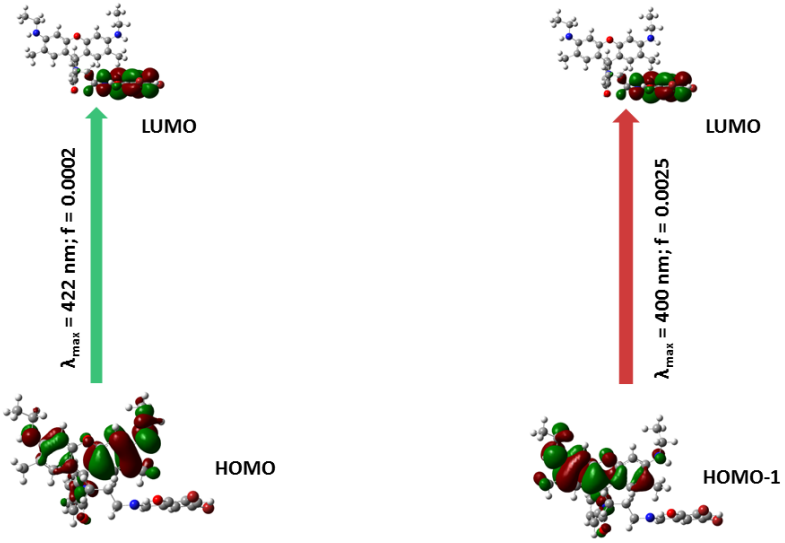

Figure S72. Pictorial representation of key transitions involved in UV-Vis absorption of chemosensor **H_3L3**.

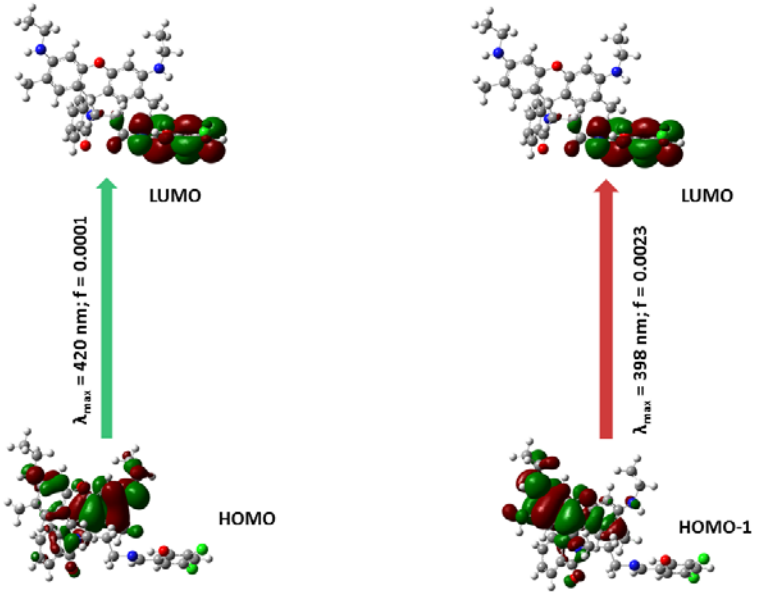

Figure S73. Pictorial representation of key transitions involved in UV-Vis absorption of chemosensor **H_3L4**.

Table S1. Crystal parameters and selected refinement details for the chemosensors (**H_3L1-H_3L4**).

Complex	**H_3L1**	**H_3L2**	**H_3L3**	**H_3L4**
Empirical formula	$C_{33}H_{30}Br_2N_4O_3$	$C_{33}H_{30}Cl_2N_4O_3$	$C_{36}H_{36}Br_2N_4O_3$	$C_{36}H_{36}Cl_2N_4O_3$
Formula weight	690.43	601.51	732.51	643.59
Temperature (K)	273(2)	273(2)	273(2)	273(2)
Crystal system	triclinic	triclinic	monoclinic	monoclinic
Space group	*P -1*	*P -1*	*P 2_1/c*	*P 2_1/c*
a (Å)	9.5600(16)	9.5793(10)	13.6753(18)	13.513(2)
b (Å)	12.335(2)	12.2135(12)	9.5139(12)	9.3806(17
c (Å)	13.635(2)	13.5543(14)	26.448(4)	25.521(5)
α(°)	92.659(4)	92.238(3)	90	90
β(°)	106.547(4)	107.023(3)	97.271(4)	94.479(6)
γ(°)	95.976(4)	96.087(3)	90	90
Volume (Å^3)	1528.1(4)	1503.7(3)	3413.4(8)	3225.2(10)
Z	2	2	4	4
D_{calc} (g cm^{-3})	1.501	1.329	1.425	1.325
Absorption coefficient (mm^{-1})	2.693	0.257	2.415	0.244
F(000)	700	628	1496	1352
θ Range for data collection (°)	27.126- 2.191	27.257- 2.322	25.08-2.98	2.286-27.285
Reflections collected	69311	49439	49611	28853
Independent reflection / R_{int}	4237/0.0845	5048/ 0.0335	2356/0.1199	5615/0.1020
Data / restraints / parameters	6741/ 0/ 396	6688/0/ 383	7514/0/414	7061/0/406
Goodness-of-fit on F^2	1.040	1.028	1.025	1.110
Final *R* indices [I>2σ(I)]	R1= 0.0678, wR2 = 0.1662	R1 = 0.0889, wR2 = 0.2717	R1 = 0.1080, wR2 = 0.2952	R1 = 0.1981, wR2 = 0.5034
R indices (all data)	R1= 0.1127 wR2 = 0.1915	R1 = 0.1093, wR2 = 0.2983	R1 = 0.2709, wR2 = 0.4043	R1 = 0.2126, wR2 = 0.5103
Largest diff. peak / hole (e Å^{-3})	1.692/ -1.177	1.351/ -0.687	1.248/ -1.204	1.001/-0.882

Table S2. Selected Bond lengths (Å) and Bond angles (°) for **H_3L1** and **H_3L2**.

H_3L1	X-ray	Calculated	**H_3L2**	X-ray	Calculated
O1-C6	1.377(6)	1.368	O1-C12	1.378(4)	1.371
O1-C18	1.383(5)	1.368	O1-C5	1.381(4)	1.371
O2-C32	1.204(6)	1.224	O3-C26	1.217(4)	1.225
O3-C11	1.321(6)	1.345	N1-N2	1.376(4)	1.355
N1-N2	1.381(6)	1.356	N1-C26	1.377(4)	1.392
N1-C32	1.384(6)	1.290	N1-C10	1.497(4)	1.513
N1-C8	1.488(6)	1.517	N2-C27	1.274(5)	1.296
N2-C9	1.256(7)	1.396	N3-C14	1.372(4)	1.387
N3-C16	1.361(6)	1.314	N3-C18	1.438(5)	1.456
N3-C15	1.438(7)	1.445	N4-C2	1.441(7)	1.456
N4-C4	1.381(7)	1.314	N4-C3	1.385(5)	1.386
N4-C2	1.455(10)	1.448	N1-C10-C6	111.5(2)	111.78
N1-C8-C19	110.9(3)	107.47	N1-C10-C11	110.6(2)	110.58
N1-C8-C26	99.4(3)	100.02	C6-C10-C11	110.7(2)	110.40
C19-C8-C26	111.6(4)	111.17	N1-C10-C20	99.4(2)	99.60
N1-C8-C7	111.5(4)	111.09	C6-C10-C20	112.5(2)	112.70
C19-C8-C7	110.9(4)	107.47	C1- C10-C20	111.7(3)	112.07
C26-C8-C7	112.1(4)	113.54			

Table S3. Selected Bond lengths (Å) and Bond angles (°) for **H_3L3** and **H_3L4**.

H_3L3	X-ray	Calculated	**H_3L4**	X-ray	Calculated
O1-C2	1.339(13)	1.332	O1-C20	1.383(11)	1.372
O2-C11	1.228(14)	1.227	O1-C21	1.407(11)	1.372
O3-C25	1.381(9)	1.372	O2-C37	1.221(13)	1.227
O3-C31	1.381(9)	1.372	O3-C3	1.340(14)	1.332
N1-C7	1.257(12)	1.281	N1-C9	1.446(13)	1.455
N1-C8	1.479(13)	1.456	N1-C10	1.497(11)	1.498
N2-C11	1.394(15)	1.382	N1-C37	1.375(13)	1.378
N2-C10	1.440(13)	1.455	N2- C14	1.376(12)	1.387
N2-C18	1.489(11)	1.498	N2-C15	1.435(15)	1.455
N3-C23	1.375(11)	1.387	N3-C25	1.379(12)	1.382
N3-C33	1.500(16)	1.459	N3-C26	1.432(13)	1.456
N4-C29	1.364(12)	1.374	N4-C5	1.245(16)	1.281
N4-C35	1.450(14)	1.456	N4-C7	1.485(15)	1.456
N2-C18 C19	112.3(6)	112.86	N1-C10-C11	110.2(7)	111.96
N2-C18 C17	99.3(7)	100.23	N1-C10-C22	111.1(7)	111.46
C19-C18-C17	111.1(7)	111.98	N1-C10-C31	101.0(7)	100.23
N2-C18-C26	110.4(7)	110.94	C22-C10-C31	111.1(8)	111.98
C17-C18-C26	112.4(7)	111.96	C31-C10-C11	112.6(7)	112.02
C19-C18-C26	110.8(7)	111.45	C22-C10-C11	110.5(7)	110.94

Table S4. Binding constant values of chemosensors in presence of Al^{3+} ions in different solvent system.

Chemosensors	Binding constant in 9:1 water: methanol (v/v) medium(M^{-1})	Binding constant in THF medium(M^{-1})
H_3L1	8.00×10^5	6.84×10^5
H_3L2	6.90×10^5	4.83×10^5
H_3L3	1.37×10^4	1.44×10^4
H_3L4	1.03×10^4	1.10×10^4

Table S5. Lifetime, quantum yield, LOD and binding constant values of chemosensors (**H_3L1-H_3L4**) and complexes (**1-4**).

	Lifetime (ns) ($\tau_{av.}$)	Quantum Yield (Φ)	LOD (nM)	Binding Constant (M^{-1})
H_3L1	3.95	0.004	-	-
H_3L2	2.56	0.003	-	-
H_3L3	1.58	0.002	-	-
H_3L4	1.06	0.004	-	-
Complex **1**	6.80	0.24	1.40	8.00×10^5
Complex **2**	4.58	0.18	2. 50	6.90×10^5
Complex **3**	4.53	0.13	4.00	1.37×10^4
Complex **4**	4.38	0.11	5.30	1.03×10^4

Table S6. Energy (eV) of selected M.O.s of chemosensors (**H_3L1-H_3L4).**

	H_3L1	**H_3L2**	**H_3L3**	**H_3L4**
LUMO+5	-0.49	-0.05	-0.24	0.03
LUMO+4	-0.61	-0.33	-0.4	-0.24
LUMO+3	-0.66	-0.39	-0.42	-0.39
LUMO+2	-1.03	-0.52	-0.44	-0.41
LUMO+1	-1.91	-0.99	-1	-1
LUMO	-2.99	-2.76	-1.7	-1.7
HOMO	-4.82	-5.34	-5.26	-5.26
HOMO-1	-6.06	-5.46	-5.37	-5.38
HOMO-2	-6.2	-5.96	-5.91	-5.91
HOMO-3	-6.57	-6.07	-6.18	-6.23
HOMO-4	-6.85	-6.58	-6.52	-6.53
HOMO-5	-6.87	-6.85	-6.83	-6.83

Table S7. Electronic transition calculated by TDDFT using B3LYP/CPCM method in water solvent of chemosensors (**H_3L1-H_3L4**).

	$E_{excitation}$ (ev)	$\lambda_{excitation}$ (nm)	Osc. Strength (f)	Key transition
H_3L1	3.48	355	0.0572	HOMO-2 ⟶ LUMO(88%)
	3.58	345	0.1152	HOMO-1 ⟶ LUMO(74%)
H_3L2	3.49	356	0.0013	HOMO-2 ⟶ LUMO(99%)
	3.58	345	0.4495	HOMO-3 ⟶ LUMO(96%)
H_3L3	3.12	422	0.0002	HOMO ⟶ LUMO(96%)
	3.35	400	0.0025	HOMO-1 ⟶ LUMO(95%)
H_3L4	3.10	420	0.0001	HOMO ⟶ LUMO (97%)
	3.35	398	0.0023	HOMO-1 ⟶ LUMO(96%)

Chart S1. Literature survey of rhodamine based derivatives used in sensing of Al^{3+}ion.

Sl. No.	Probe	Crystal Structure	Sensing of metal ion(s)	Excitation(nm)/ Emission(nm)	Sensing Media	Binding constant	Limit of detection (LOD)	Biological study	Refs.
1.	**pyrazole-based chemosensor (Pry-R6G)**	No	Al^{3+}	532/568	(DMF/H_2O, 1/99, v/v)	-	2.61×10^{-8} M	No	**44a**
2.	**rhodamine B-2-chloronicotinaldehyde derivative (RBCN)**	No	Al^{3+}	560/584	CH_3CN	2.96×10^{-5} M^{-1}	2.86×10^{-8} M	No	**44b**
3.	**3′,6′-Bis(diethylamino)-2-(2-isothiocyanatoethyl)spiro-[isoindoline-1,9′-xanthen]-3-one (2)**	No	Al^{3+}	554/583	CH_3CN:H_2O (1:1, v/v)	4.5×10^{-4} M^{-1}	1.1×10^{-8} M	No	**44c**
4.	**1,2,3-triazole-ringappended rhodamine dye (L)**	No	Al^{3+}	540/577	CH_3OH-H_2O, 9:1 (v/v)	2.55×10^4 M^{-1}	-	No	**44d**
5.	**2-(2-((3-(tert-butyl)-2-hydroxybenzylidene)-amino)ethyl)-3′-6′-bis(ethylamino)-2′,7′-dimethylspiro-[indoline-1,9′-xanthen]-3-one (HL-t-Bu)**	Yes	Al^{3+} and Zn^{2+}	500/550 370/457	10 mM HEPES buffer (methanol/water mixture) (9:1, pH = 7.4)	9.38×10^3 M^{-1} and 4.75×10^4 M^{-1}	10.98×10^{-9} M and 76.92×10^{-9} M	Yes	**44e**
6.	**3′, 6′- bis(diethylamino)-2-(2-((2-((2-hydroxybenzylidene)amino)phenyl)thio)ethyl) spiro[isoindoline 1,9′ xanthen]-3-one (L)**	Yes	Al^{3+} and Hg^{2+}	388/485 525/585	HEPES-buffered (20 mM, MeOH/H_2O, 4/1, v/v, pH 7.4)	4.66×10^6 M^{-1} -	0.005×10^{-6} M and 0.05×10^{-6} M	Yes	**44f**
7.	**(3-(3,5-dimethyl-pyrazol-1-ylmethyl)-2-hydroxy-5-methyl-benzaldehyde (HL^5)**	No	Al, Fe and Cr	510/555 510/555 510/555	methanol/H_2O (1 : 1, v/v, pH 7.2)	8.2×10^4 M^{-1}, 6.7×10^4 M^{-1} and 6.0×10^4 M^{-1}	0.34×10^{-6} M , 0.29×10^{-6} M and 0.31×10^{-6} M	Yes	**44g**
8.	**rhodamine-based derivative (L)**	Yes	Al^{3+}	500/556	H_2O–EtOH (4 : 1, v/v)	3.14×10^5 M^{-1}	3.26×10^{-6} M	Yes	**44h**
9.	**(E)-3',6'-bis(diethylamino)-2-(2-(pyren-4-ylmethyleneamino)ethyl)spiro[isoindoline-1,9'-xanthen]-3-one (L)**	Yes	Al^{3+}	400/586	HEPES buffer (0.1 M; EtOH–H_2O, 4 : 1 v/v; pH 7.4	1.19×10^4 M^{-1}	0.02×10^{-6} M	Yes	**44i**
10.	**3′,6′-bis(ethylamino)-2-(2-(2-hydroxy-5-methylbenzylideneamino)ethyl)-2′,7′-dimethylspiro[isoindoline-1,9′-xanthen]-3-one (HL-Me)**	Yes	Al^{3+}	500/552	10 mM HEPES buffer, pH 7.4, H_2O/MeOH = 1 : 9 (v/v)	2.05×10^5 M^{-1}	2.8×10^{-9} M	Yes	**44j**

11.	**rhodamine Schiff base (L)**	Yes	Al^{3+}	525/590	HEPES buffer (1 mM, pH 7.4; EtOH–water, 1 : 3 v/v)	8.13 $\times 10^4$ M^{-1}	60 $\times 10^{-9}$ M	Yes	**44k**
12.	**Rhodamine-diformyl p-cresol conjugate (L)**	No	Al^{3+}	460/585	HEPES-buffered (0.1 M) EtOH:water (4:1, v/v), pH 7.4	9.1 $\times$ 10^6 M^{-2}	5 $\times 10^{-9}$ M	Yes	**44l**
13.	**2-((3,5-dibromo-2-hydroxybenzylidene)amino)-3',6'-bis(ethylamino)-2',7'-dimethylspiro[isoindoline-1,9'-xanthen]-3-one, (HL1)**	Yes	Al^{3+}	490/555	10 mM HEPES buffer, pH 7.4, (H_2O/MeOH) (9:1 v/v)	8.00$\times 10^5$ M^{-1}	2. 50 $\times$ 10^{-9} M	Yes	**This Work**
14.	**2-((3,5-dichloro-2-hydroxybenzylidene)amino)-3',6'-bis(ethylamino)-2',7'-dimethylspiro[isoindoline-1,9'-xanthen]-3-one, (HL2)**	Yes	Al^{3+}	490/555	10 mM HEPES buffer, pH 7.4, (H_2O/MeOH) (9:1 v/v)	6.90$\times 10^5$ M^{-1}	1.40 $\times$ 10^{-9} M	Yes	**This Work**
15.	**2-(3-((3,5-dibromo-2-hydroxybenzylidene)amino)propyl)-3',6'-bis(ethylamino)-2',7'-dimethylspiro[isoindoline-1,9'-xanthen]-3-one, (HL3)**	Yes	Al^{3+}	490/555	10 mM HEPES buffer, pH 7.4, (H_2O/MeOH) (9:1 v/v)	1.37$\times 10^4$ M^{-1}	0.053 $\times$ 10^{-9} M	Yes	**This Work**
16.	**2-(3-((3,5-dichloro-2-hydroxybenzylidene)amino)propyl)-3',6'-bis(ethylamino)-2',7'-dimethylspiro[isoindoline-1,9'-xanthen]-3-one, (HL4)**	Yes	Al^{3+}	490/555	10 mM HEPES buffer, pH 7.4, (H_2O/MeOH) (9:1 v/v)	1.03 $\times 10^4$ M^{-1}	0.040 $\times$ 10^{-9} M	Yes	**This Work**